Development of a real time quality monitoring device for resistance spot welding

Wong, Yoke Rung

2008

Wong, Y. R. (2008). Development of a real time quality monitoring device for resistance spot welding. Master’ s thesis, Nanyang Technological University, Singapore.

https://hdl.handle.net/10356/5395

https://doi.org/10.32657/10356/5395

Nanyang Technological University

NANYANG TECHNOLOGICAL UNIVERSITY

DEVELOPMENT OF A REAL TIME QUALITY MONITORING DEVICE FOR RESISTANCE SPOT WELDING

WONG YOKE RUNG

SCHOOL OF MECHANICAL & AEROSPACE ENGINEERING

2008

DEVELOPMENT OF A REAL TIME QUALITY MONITORING DEVICE FOR RESISTANCE SPOT WELDING WONG Y.R. 2008

DEVELOPMENT OF A REAL TIME QUALITY MONITORING DEVICE FOR RESISTANCE SPOT WELDING

WONG YOKE RUNG

School of Mechanical & Aerospace Engineering

A thesis submitted to the Nanyang Technological University
in fulfilment of the requirement for the degree of
Master of Engineering

2008

ABSTRACT

Resistance Spot Welding (RSW) is a broadly used material joining method. To ensure the integrity of product, many quality monitoring methods involved both destructive (DT) and non-destructive testing (NDT) have been developed over the years. However, these testing are either difficult to use, offline operation or low efficiency, making it impossible to provide the instant and accurate information regarding the weld quality. In this research, a recently developed monitoring technique was presented by using electrical input impedance (Z_{in}) as monitoring signature. This single frequency, time variant signature, was easily obtained by measuring and processing the input current and voltage from welding circuit during the welding process. It was found that the relationship of Z_r, which was the real part of Z_{in}, was capable to correlate with the welding strength. This correlation was done by employing a pattern recognition and classification system with an artificial neural network (ANN). After the training of ANN was completed, the result showed that the weld quality was 100% distinguished and subsequently a real time quality monitoring system was proposed. Beside that, various weld operating parameters and process conditions like pressure, welding current, electrode and angled weld have been examined so that their relationships with the features of Z_r and hence the welding strength could be further confirmed. It was observed that the Z_r deviated obviously according to the changes of these factors and lower welding strength were caused by low welding current and side damage of electrode. Additionally, the seriousness of weld expulsion was also observed and it could be clearly reflected by the Z_r. For the in-situ

study of RSW, microstructure of RSW examined by Scanning Electron Microscope (SEM) and optical microscope were presented and then correlated with the Z_r successfully. With the above results, the features of Z_r like alpha peak, throat, beta peak and sudden drop of Z_r were identified to be important in pattern recognition and the characterization of Z_r was also done with respect to the nature of RSW.

ACKNOWLEDGEMENT

Firstly, I would like to thank my supervisor, Professor Ling Shih-Fu for his guidance, help and support in my research. Without him, this report couldn't be completed.

Secondly, I also want to thank the technicians and research students in Mechanics of Machines Lab, Center for Mechanics of Micro-systems, Service Workshop A and Material Lab A where they provide me a good environment so that I can focus to do my research smoothly.

Lastly, I would like to also thank my families, especially my wife, Xing Xuan, for their continuous and unconditional encouragements and cares.

TABLE OF CONTENTS

LIST OF FIGURES

LIST OF TABLES

NOMENCLATURE

ROMAN SYMBOLS

A	Cross section area, m^2
C	Capacitance, F
d	Diameter of weld nugget, m
H	Joule heating, J
I	Weld current, A
L	Inductance, H
l	Length or thickness, m
R	Resistance, Ω
T	Time, s
t	Thickness of metal sheet, mm
V	Voltage, V
Z_{in}	Input impedance, Ω
Z_r	Real part of Z_{in}
Z_x	Imaginary part of Z_{in}

GREEK SYMBOLS

ϕ	Phase shift, rad
ρ	Electrical resistivity, Ωm
ω	System frequency, Hz
Φ	Inclined angle, º

CHAPTER 1

INTRODUCTION

This chapter will first introduce the background and motivation of this research work followed by the objectives and scope of work. The construction of the thesis will also be presented at the end of the chapter.

1.1 Background

Resistance Spot Welding (RSW) is widely used in sheet metal fabrication due to its advantages such as easy to use, low cost, clean working environment and short process time. The RSW is referring to the welding process whereby the heat is generated by the resistance of metal sheets being welded to the flow of very high electric current. The welding current, usually is as high as a few thousands amperes, is achieved via the transformer, which converts the low current from the primary circuit to the high current in secondary circuit. Apart from this, pressure is applied on the sheet metals through the electrodes to ensure the adequate contact between the interfaces of sheet metals. The basic configuration of RSW is shown in Fig. 1.1.

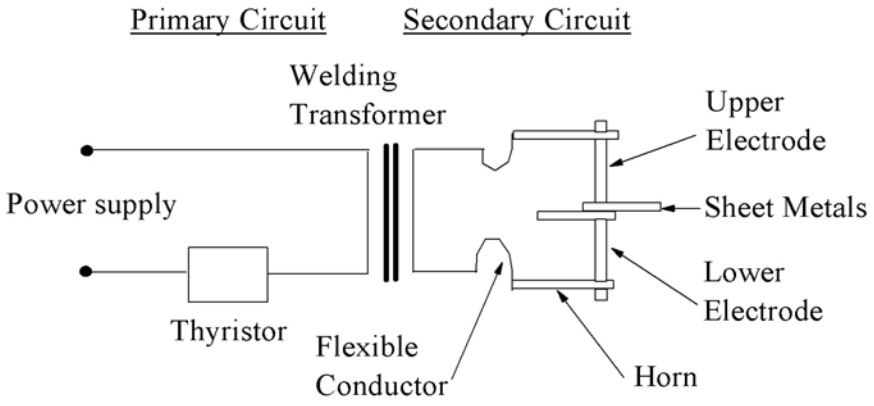

Figure 1.1 Configuration of a welding circuit.

For the past decades, the RSW is heavily used in automobile, transportation and appliance industries. For an example, there are thousands of spot welds on a car body. The quality of RSW becomes a major concern for the product because it directly affects not only the structural integrity but also other quality issues such as anti-corrosion, vibration, noise and etc. Generally, appearance of weld and welding strength are the criteria used for judging the weld quality. The first criterion is always subjective and it depends on individual customer's need. However, the welding strength is governed by international standard such as the one established by Resistance Welding Manufacturing Alliance (RWMA). It is referring to the fracture force measured during shearing test or cross-tensile test. These mechanical tests are destructive testing (DT) because the workpieces are destroyed after testing. As the joining strength is closely related to the weld nugget dimension, the average diameter of weld nugget is often used as the criteria because of convenience. RWMA Standard, for example, provides a table [Appendix A] to correlate the weld nugget dimension with welding strength so that quality checking is done faster.

Although the RSW process is controlled by many process conditions and operating parameters, controlling these factors does not guarantee the welding conditions and thus the weld quality. It is therefore necessary to develop a quality monitoring method to ensure the weld quality in manufacturing environment. Mechanical DT is not suitable for obvious reasons: time consuming, expensive, low productivity and off-line monitoring. To overcome these restrictions, various non-destructive testing (NDT) methods have been attempted. As an ideal quality monitoring method, it should satisfy the following criteria:

(1) Real-time (Decision made on site before next welding starts).

(2) In-situ (No welding parameters are affected or changed).

(3) Accurate.

(4) Cost effective.

Unfortunately, most of existing methods found in literature fails to satisfy all these criteria.

In this research, a newly established method, which is based on the measurement of the input electrical impedance (Z_{in}) of RSW, is employed as a NDT technique to develop a real-time quality monitoring method. By measuring the input current and voltage from the secondary circuit, the Z_{in} of corresponding spot weld can be found in real time. This complex time-varying quantity contains rich information about the physical changes

happening during the welding process. It therefore can serve as a good monitoring and diagnosis signature for the weld quality.

1.2 Research Objectives and Scope

This research work aims to develop a real time quality monitoring method for RSW based on Z_{in}. It means to establish a deep understanding on the relationships between Z_{in} and welding parameters, conditions and quality of a RSW process. More specially, the research objectives further includes:

(1) To correlate the Z_{in} to the weld quality by going through a pattern classification system.

(2) Designing the proper operating flowcharts as the fundamental of developing a compact size, real-time and online monitoring device for RSW.

(3) To study in-situ about the Z_{in} with microstructure change of RSW.

Fig. 1.2 presents all relevant factors which results in a weld quality and thus further elaborates the features of the research.

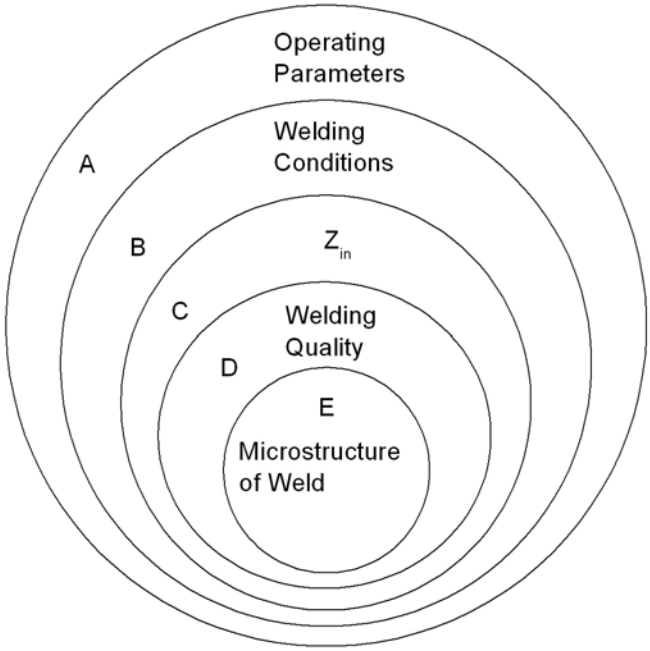

Figure 1.2 Scope of work.

Since the measurement of Z_{in} is easy, fast, real-time and in-situ, it becomes a simple and yet efficient tool for studying the RSW in many aspects. For instance, by having the Z_{in} in the medium layer (C), the welding quality (D) and microstructure of weld (E) can be studied effectively because they can be correlated firstly to the operating parameters (A) and welding conditions (B) via Z_{in}. Any variation of Z_{in} waveforms should be able to reflect the weld quality and changes of microstructure instantly. Therefore, a lot of tedious work such as performing mechanical tests and specimen preparation for metallurgy study of welding can be avoided. Furthermore, its capability can be significantly enhanced by employing an automation system. Artificial Neural Network (ANN) is a good choice to automate such system.

In order to achieve all the benefits of Z_{in} mentioned above, several tasks have to be completed. Investigation on the effects of A and B to C is carried out through experimental work. For the following stage, the most important operating parameter is selected to correlate with C. At the meantime, the weld strength is also measured by performing mechanical test so that the weld quality can be monitored automatically by the established system. With the help of scanning electron microscope (SEM) and optical microscope, the microstructure changes of RSW can be studied by taking high magnified metallurgical images on welded surface and hence correlated with C.

1.3 Organization of Report

This thesis consists of 7 chapters. Chapter 1 generally gives introduction, background and the scope of the research work. Chapter 2 reviews literature regarding the fundamental of RSW, welding quality criteria, and existing quality monitoring techniques. Chapter 3 deals with the fundamental of Z_{in} including its definition, physical meaning of Z_{in} in RSW, and its measurement and calculation. A case study of weld quality using impedance is included to illustrate its general application. Chapter 4 reports how to automate an automated weld quality monitoring system based on Z_{in}. In this chapter, features of the Z_{in} waveforms are selected and then an ANN is introduced to recognize the patterns of Z_{in} waveforms. Furthermore, a conceptual design of automatic weld quality monitoring product is also presented. In Chapter 5, the relationship between Z_{in} with major operating parameters and abnormal process condition are reported. For in-situ study of RSW, the correlation of Z_{in} with the microstructure change of RSW is presented

in Chapter 6. Finally, the important findings, conclusions and future prospects are drawn in Chapter 7.

CHAPTER 2

INTRODUCTION AND LITERATURE REVIEW

In this chapter, the working principle and commonly adopted equipment of RSW process is introduced. It is then followed by a discussion on judgment of weld quality such as welding strength, weld appearance and weld nugget dimension. This chapter is then ended by summarizing the existing destructive testing and non-destructive testing for RSW.

2.1 Mechanism System of RSW

Resistance Spot Welding has been widely used in modern industrial applications since it was invented by Elihu Thompson in 1877 [1]. The application of RSW is mainly found in car industry due to the advantages [2]:

(1) Producing strong welds on sheet metal such as low carbon steel and etc.

(2) Low initial cost and no consumables such as wires, rods, or gas are required.

(3) Clean, smoke or fumes free.

(4) Fast welding times of 1 second or less.

(5) Finishing work is minimized because there is no weld metal to grind down.

(6) High robustness and flexibility due to a full range of interchangeable arm sets for welders are available.

As shown in Fig. 2.1, a single phase power supply is connected to provide 50Hz electric power. A welding transformer is used to step down the voltage and largely increase the current. Heat is generated by the resistance of the parts being welded and the flow of electric current, to melt the metal at faying interface (sheet to sheet interface) adequately. The product of RSW is a metallic joint called "weld nugget". Pressure is applied through the electrodes to ensure the intimate contact between the metal sheets throughout the process. The two copper alloys electrodes are normally water cooled so that the electrode to sheet interface is cooled down to prevent sticking.

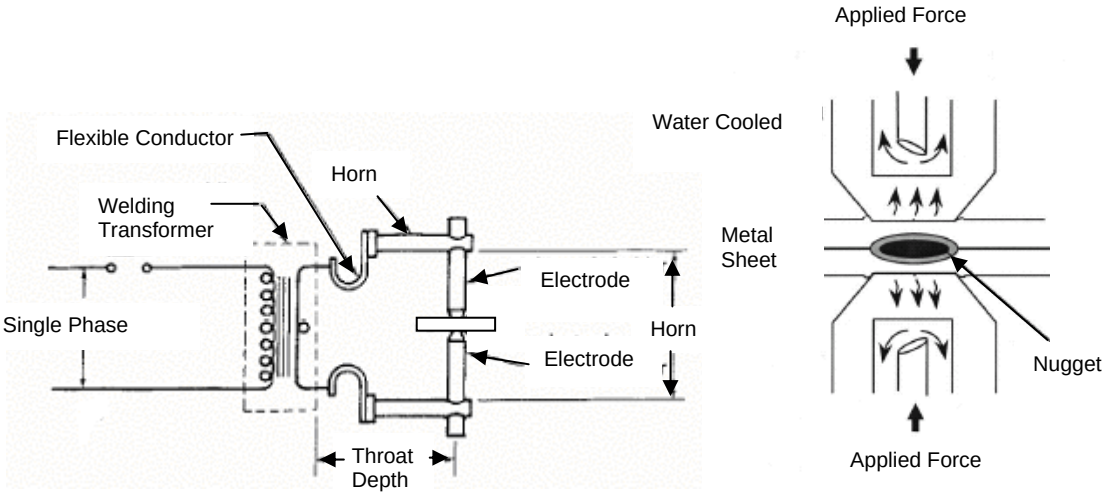

Figure 2.1 Schematic diagram of resistance spot welding.

In theory, RSW is a mechanical-electrical-thermal coupled process. The weld nugget can be seen as a result due to heat generated as a function of welding current, welding time

and electrical resistance of the workpieces. The relationship can be described by Joule's law.

$$H = I^2RT \tag{2.1}$$

where H: Joule heating (J);

I: Welding current (A);

R: Resistance (Ω);

T: Weld time (s);

To effectively generate heat in a short time, the welding current is made very high, the welding time short. Besides providing adequate heat to melt metal sheet, it also associates with heat losses such as heat dissipation due to the water cooled electrodes, heat convective to the air and conductive to the base metal.

As shown in Fig. 2.2, a RSW process is formed by three operating stages in sequence:

(1) Squeeze stage: The electrodes are in contact with the workpiece when the pressure is applied.

(2) Welding stage: The electric current flows through the system. Fusion of the workpiece occurs during this stage.

(3) Holding stage: The current flow is shut off and the pressure is constantly applied until the end of hold time. During this stage, the weld nugget starts to solidify rapidly. The pressure at holding time is to ensure an enhanced mechanical property of the weld nugget.

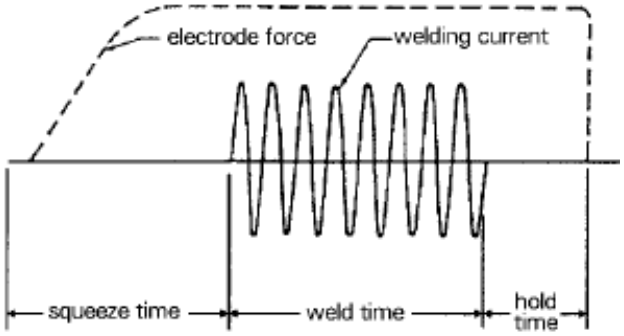

Figure 2.2 Resistance spot welding process.

2.2 Operating Parameters for RSW

There are various operating parameters for RSW due to the interaction between the complex workpiece and the coupled process. In Fig. 2.3, these operating parameters are clustered into 5 major parameters: (a) Welding current; (b) Welding time; (c) Pressure; (d) Electrode; (e) Material. In the following, discussions are given to each in detail.

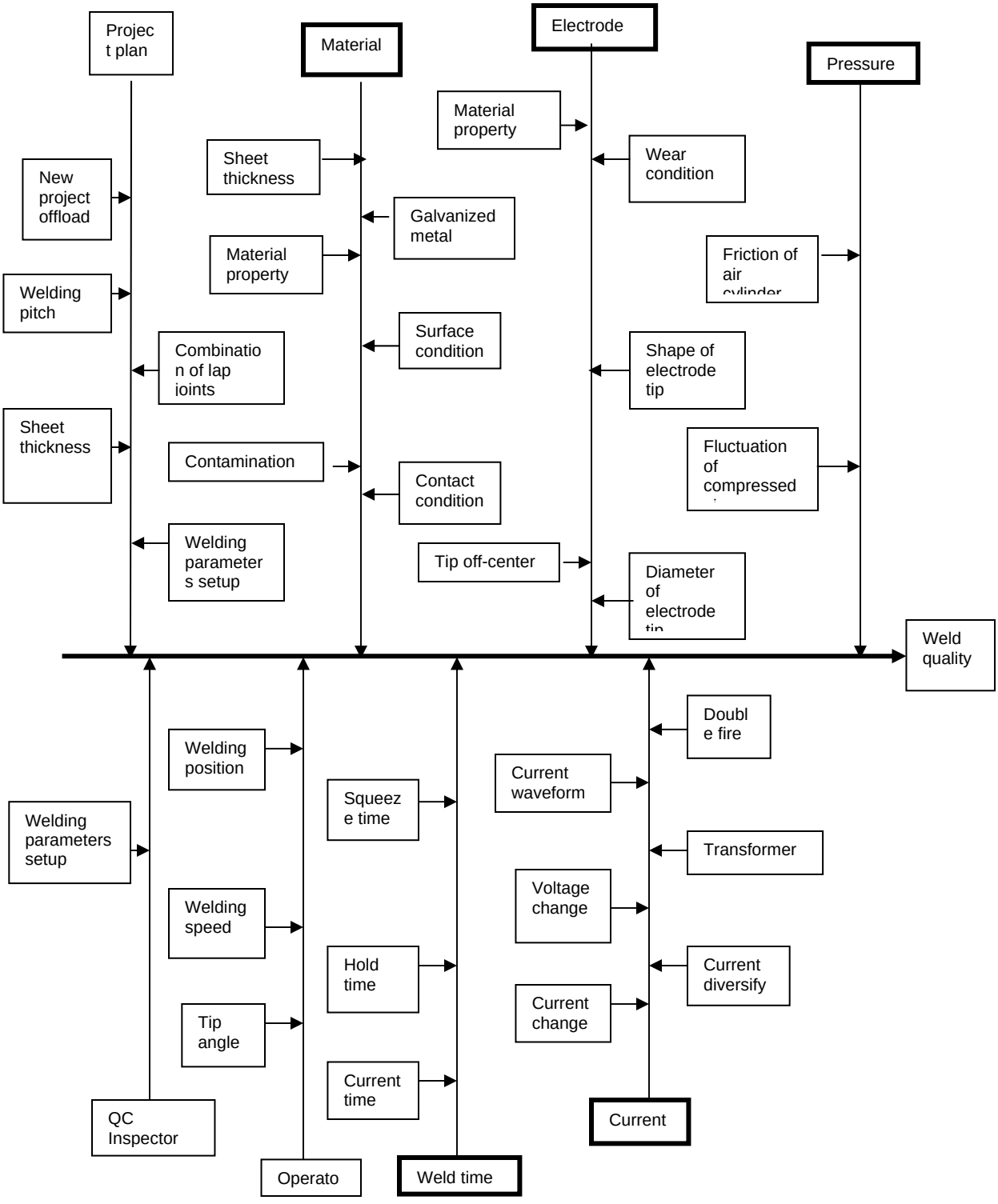

Figure 2.3 Fish skeleton analysis for the factors of RSW (Courtesy of China Motor Corporation).

2.2.1 Welding Current

From Eq. (2.1), it is observed that the heat generated is proportional to the square of current. Therefore, a little change in current may lead to over-heating or under-heating of the weld nugget. Bowers *et al.* [3] constructed a mathematical model to study the effect of the electrode geometry on current distribution. It revealed that the electrode geometry shifted the current distribution and subsequently caused a localized wear of electrode surface if the electrode geometry was not properly designed. This was important because the localized wear would lead to the deterioration of electrode and hence shortened its lifespan.

Even on the intimate contact area, the current density is not evenly distributed due to the electrode geometry. Fig. 2.4 shows that the current density is higher at the edge and becomes relatively uniform towards the center of electrode. Theoretically, the ratio of electrode diameter to the thickness of workpiece affects the current distribution. The larger ratio is created, the more uniform current distribution will be.

The change of temperature distribution also affects the current density throughout the welding process. The electric resistance increases when the temperature is rising. However, the current density reduces in the center of weld nugget where the temperature is always very high and shifts to the surroundings of nugget. Fig. 2.5 illustrates the current distribution at the nugget and its surroundings.

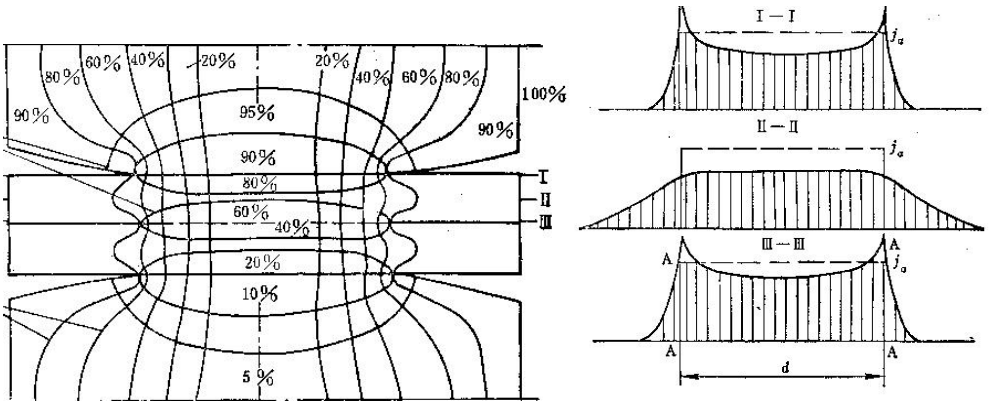

(a) (b)

Figure 2.4 (a) Electric field distribution; (b) Current density during welding process at interfaces: I, Electrode/Sheet; II: bulk metal; III: Sheet/Sheet.

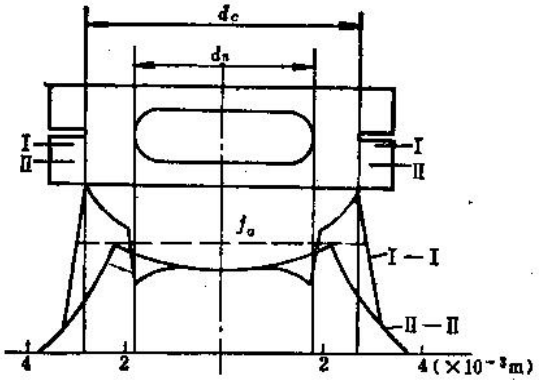

Figure 2.5 Current distribution along the center of weld nugget.

2.2.2 Welding Time

Most of RSW is completed in a very short time period, usually less than 1s. Based on Fig. 2.2, a complete cycle of welding process consists of squeeze time, current time, holding time and off time. The squeeze time is the time between the pressure is applied and welding. An electric current starts to flow through the system during current time. The

contact resistances and current path are established and the formation of weld nugget also takes place during this period time. After the current is cut off, the electrodes still hold their position to facilitate further solidification of weld nugget within holding time. Finally, the electrodes release for the next weld set by off time.

2.2.3 Pressure

The purpose of pressure is to bring the workpiece in contact and hold them in intimate contact at the welded surface. This action ensures consistency and conductivity at all the interfaces. Also known as electrode force, the pressure is applied to the workpiece by following the sequence as shown in Fig. 2.2.

The electrode force is suspected to affect the resistances. In the research work done by Song *et al.* [4], he has explained about the influence on contact resistance by pressure and other parameters. The results showed that the influence of pressure was quite consistent for different materials and the contact resistance decreased when the electrode force increased. In literature review [5], it was reported that the low electrode force would result into higher contact resistance. Furthermore, a low electrode force will cause the expulsion of weld during welding process because it is unable to retain the molten metal in the fusion region, which is enclosed by the solid metal. The weld quality can be affected by high electrode force too. The excessive electrode force is suspected to cause the reduction of initial heating and average current density, which results in a smaller weld nugget and therefore weaker welding strength. The life span of electrode will also

be shortened by the increasing force due to the severe deformation of tip surface of electrode.

2.2.4 Electrode

The function of electrode is to create a current flow path and apply the electrode force to the welded surface. Most of the electrode is made of copper alloys. They are the only consumable parts for RSW. In order to prevent the electrodes from sticking on the metal sheet and severe deformation of tip surface, the electrode is water cooled to lower down the temperature at the electrode to sheet interface and itself.

There are two types of electrode based on the different designs on the electrode tip (Fig. 2.6). However, it is rarely to use the round head type due to its small and inconsistent contact area. In 1990, Bowers *et al.* [3] studied about the truncated cone electrode and its modified type, pimple tip. This electrode was actually a circular cylinder with a step down diameter at the tip surface. He found out that the current distribution was more uniform for bigger *a* angle of truncated cone. This result was confirmed by the pimple tip type that having the same shape of electrode. Despite of the uniform current distribution, it sacrificed the mechanical strength and heat dissipation, which caused shorter life span of electrode. Later in 1999, Yeung *et al.* [6] introduced a model to describe the transient thermal in electrode and the effect of water flow rate to the electrode cooling. These factors were important because the lifespan of electrode could be shortened if they were

not properly controlled. Fukumoto *et al.* [7] also reported the causes of electrode degradation and subsequently affected the weld quality.

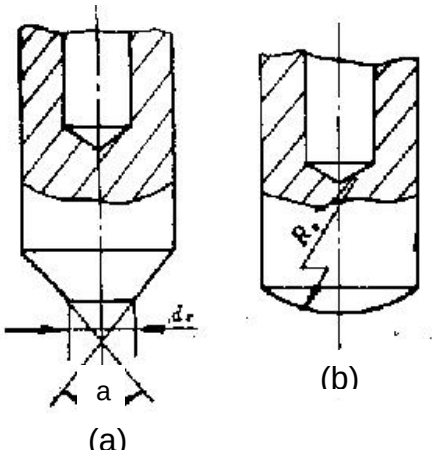

Figure 2.6 (a) Truncated cone type; (b) Round head type of electrode.

2.2.5 Material

The material used for the manufacturing of metal sheets becomes more and more complicated and challenging in terms of material property, surface treatment and thickness. For the past decades, many research works have been done in order to improve the mechanical performance such as strength, weight, fuel efficiency and productivity. All these improvements require advanced material property, surface treatment and manufacturing technology. Traditionally, only low carbon steel is used but other materials such as Aluminum, Zinc coated steel and high strength steel are also common and important due to their advantages in terms of physical and mechanical property.

According to Howard's definition, the weldability of metal is "the ease with which a satisfactory weld can be made that will produce a joint equal to the metal being welded" [8]. Based on this definition, it is known that most of metals are weldable but only some metals are much more difficult to weld in terms of welding process and welding procedure. Therefore, the metal must be considered based on its physical and mechanical property before welding. Both physical and mechanical properties of metal are shown in Table 2.1 and 2.2.

Table 2.1 General physical properties of metal.

Physical Property	Definition
Melting Point	The temperature when the metal changes from a solid state into a liquid state.
Boiling Point	The temperature at which the metal changes from the liquid state to vapor state.
Thermal Conductivity	The ability of metal to transmit heat throughout the domain. Generally, a metal can conduct heat away from the spot weld area faster than the other.
Specific Heat	The amount of energy required to raise the temperature of 1 gram of metal 1 ºC. It indicates the amount of heat required to bring the metal to its melting point.
Thermal Expansion	The coefficient of linear thermal expansion measures the linear increment per unit length based on the change in temperature.
Electrical Conductivity	The capacity of metal to conduct an electrical current in micro-ohms per cubic centimeter at 20 ºC.

Table 2.2 General mechanical properties of metal.

Mechanical Property	Definition
Strength	The ability to withstand the external force without mechanical failure taking place.
Ductility	The ability to be stretched without breaking and to retain the changed shape after the load has been removed.
Hardness	The hardness of a metal is measured by a hardened steel ball put onto the surface and shown as Brinell hardness number (BHN).

As mentioned earlier, the surface treatment also plays an important role for RSW. It refers to the cleanliness process on the surface of sheet metal. In actual manufacturing environment, the surface of sheet metal is always contaminated by mechanical oil, water, oxidized layer, dust and etc. These contaminants may affect the contact resistance of the sheet metal and hence the weld quality. For normal practice in laboratory, the contamination is usually removed by using ultrasonic bath containing chemical solution. Additionally, some other methods such as mechanical polishing (by sand paper or grinding machine) are also included for more complicated surface treatment process.

2.3 Electrical Resistance in RSW

The RSW is a coupled electrical-thermal-mechanical system. From Eq. (2.1), one can understand the importance of resistance in the process as the heat generation depends on the resistance. Fig. 2.7 shows the number of electrical resistances in series [5]. The total

resistance consists of two parts, which are bulk resistance and contact resistance. R1, R3, R5 and R7 are bulk resistance whereby R2, R4 and R6 are contact resistance.

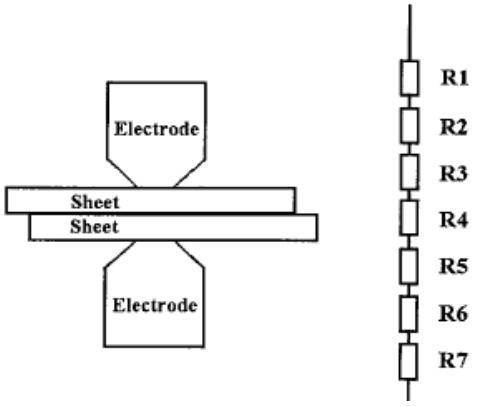

Figure 2.7 Important electrical resistances in a welding process.

2.3.1 Bulk Resistance

The bulk resistance refers to the electrical resistivity of a metal, which can be expressed as:

$$R = \frac{\rho * l}{A} \tag{2.2}$$

where R: Bulk resistance (Ω);

ρ : Electrical resistivity (Ωm);

A: Cross section area (m^2);

l: Length or thickness (m);

The electrical resistivity of metal is depended on the temperature. As the temperature of metal increases, the resistance also increases. It is obvious that the bulk resistance changes according to the thermal cycle for every weld made and hence it is potentially used to indicate the temperature distribution of base material or electrode.

2.3.2 Contact Resistance

From the microstructure of metal, the surface of sheet metal is determined by surface roughness, which indicates that its surface is not perfectly flat. As shown in Fig. 2.8, it is observed that the contact at the faying interface is actually partial contact over the welded surface. How does this partial contact form is depended on the applied pressure. Experimental result showed that the contact resistance was inversely proportional to the applied force [4]. Additionally, the contamination on the surface such as mechanical oil also alters the surface condition and subsequently causes inconsistency of contact resistance.

Since the factors such as temperature and contact surface condition cannot be sustained constantly throughout the welding process, the summation of bulk and contact resistance is therefore known as “dynamic resistance”.

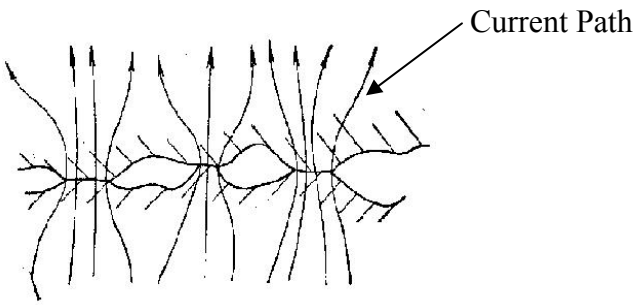

Figure 2.8 Contact condition at the faying interface.

2.4 Formation of Weld Nugget

In general, the weld nugget is the product of RSW. Fig 2.9 shows a typical weld nugget formed for single lap joint. The formation of weld nugget is depended on all the operating parameters and process conditions mentioned in this chapter. The formation of weld nugget is vital important because it directly influences the weld quality. Basically, it can be summarized into 2 major aspects to describe the formation of weld nugget.

2.4.1 Temperature Distribution and Formation of Weld Nugget

Temperature distribution refers to the different temperature points at the locations in the weld region. Fig. 2.10 shows the temperature distribution along Z-axis of the weld region with respect to the initial and final welding process. The temperature distribution is important in analysis of weld formation because it provides rich information for the heat generation and hence the weld nugget growth.

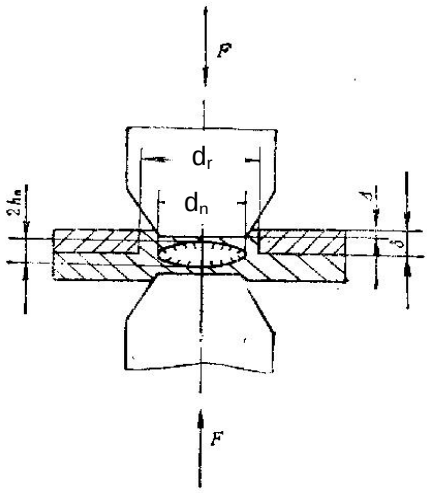

Figure 2.9 Formation of weld nugget, d_r is diameter of heat-affected-zone; d_n is diameter of weld nugget.

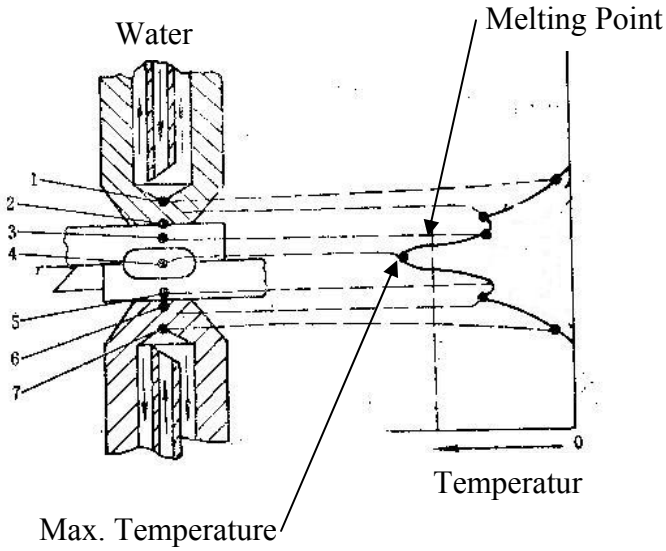

Figure 2.10 Temperature distribution along the z-axis of weld region.

2.4.2 Dynamic Resistance and Growth of Weld Nugget

As mentioned earlier, the summation of bulk and contact resistances is truly varying and known as dynamic resistance. Basically, it can be obtained by dividing the peak or RMS

value of each half cycle of the measured voltage and its corresponding current [9] [10]. In 1987, Gedeon *et al.* [11] improved its accuracy by representing each half cycle of the voltage and current with a curved line. Furthermore, Cho *et al.* [12] pointed out that dynamic resistance could be obtained from the primary circuit instead of secondary circuit. Wang *et al.* [13] also proposed a mathematic model to analyze the dynamic resistance by taking the sum of temperature-dependent bulk resistance of workpiece and the contact resistances.

The relationship between the shape of the dynamic resistance curve and the formation of weld nugget for uncoated steels is established by Williams *et al.* [5]. Fig. 2.11 shows how does the dynamic resistance curve develop with respect to time. Initially, the resistance decreases rapidly to its minimum due to the breakdown of surface asperities. It increases to a peak resistance as the temperature is increasing. During this period, the base metal starts to melt once its melting point is reached. The molten metal grows rapidly while the resistance is peak again as a compromise between the increment of resistance due to bulk heating and the decrement of resistance due to the molten metal continues to grow. After that, the total resistance decreases as the current path is shortened due to the indentation of sheets.

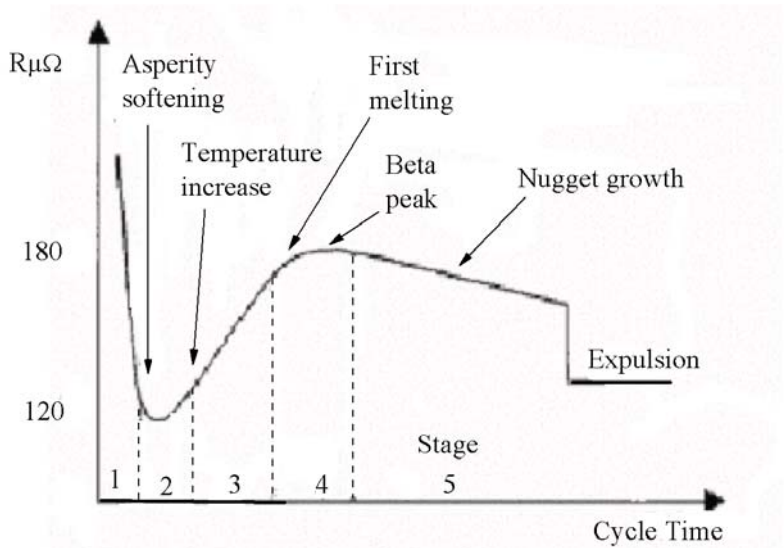

Figure 2.11 Dynamic resistance curve for uncoated steel.

2.5 Quality of RSW

The quality of RSW has direct impact on the quality of product in terms of strength, anti-corrosion and etc. Generally, the quality of RSW refers to 2 major components: (1) appearance of weld; (2) welding strength. There is a wide room left for the first criteria because individual party may have different requirements. For example, some may require lesser burnt mark or indentation but some may not. In this situation, the weld quality judgment has not been standardized. However, the international standard such as Resistance Welding Manufacturing Alliance (RWMA) and Japanese Industrial Standards Committee (JISC) has been established in order to govern the welding strength because it is more importantly related to the impacts of quality as mentioned above. Since they are interrelated to each other, only RWMA Standard will be discussed.

Basically, RWMA Standard shown in Appendix A provides a table to show the relationship between the operating parameters, welding strength and weld nugget dimension. For the welding strength, it reflects the ability of weld to withstand the design load without mechanical failure. According to British Standard [14], this welding strength can be obtained by performing shear or cross-tension tests (as shown in Fig 2.12). After the workpiece is being destroyed, the measured fracture force is compared with Class A, B or C, which are shown in RWMA Standard, to examine its quality.

For convenience purpose, the fact that weld strength is closely related to weld nugget dimension and the later is included in the above-mentioned table to determine the weld quality. In Fig. 2.13, the weld nugget dimension is estimated based on average weld nugget diameter. Since the measurement does not require any precise equipment and yet provide a good reference for weld quality, it has been widely used as a quick reference in industry. Despite of this advantage, the weld nugget dimension cannot be the final quality judgment because it is unable to reflect the problems such as loose weld and over weld. Therefore, the welding strength still dominates the quality judgment as it provides an accurate and reliable result of destructive testing. Because of this reason, the welding strength measured by tension test will be used as the reference of weld quality judgment in this thesis.

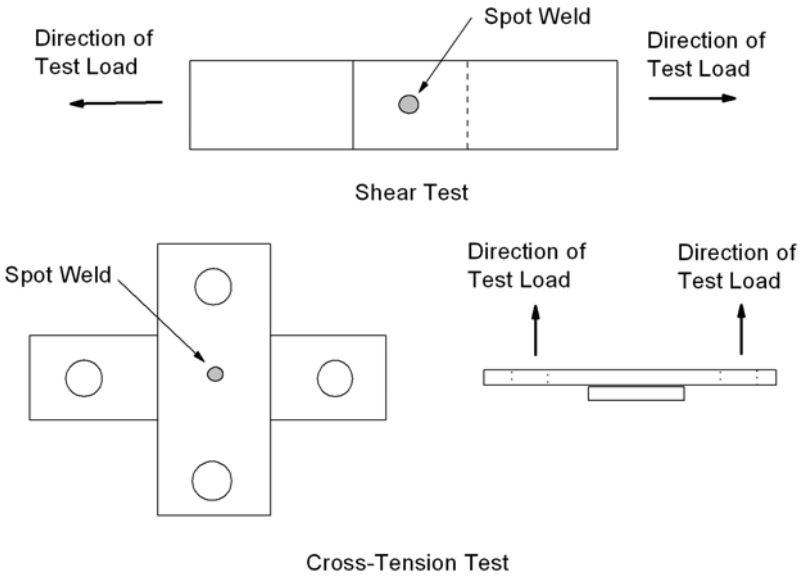

Figure 2.12 Welding strength testing.

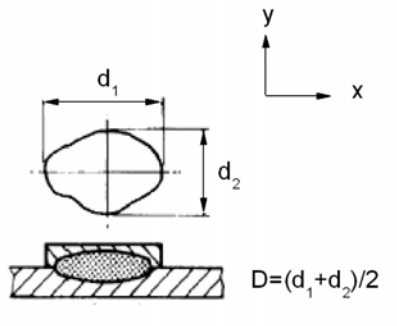

Figure 2.13 Measurement of weld nugget dimension.

2.5.1 Destructive Evaluation of Weld Quality

Destructive testing (DT) is a conventional method that has been used for the past decades. The advantages of this method are simple and easy to apply. The commonly used DT methods are tension test, cross-tension test, peel test, twist test and chisel test. For the first two methods, it has been described in the section above and the major purpose is to

obtain the welding strength. Besides that, by performing the peel or twist test, the workpiece is either peeled or torn apart in order to measure the weld nugget dimension. However, a semi-destructive method known as chisel test is also used as shown in Fig. 2.14. Basically, the deformed portion of the workpiece is repaired after the inspection.

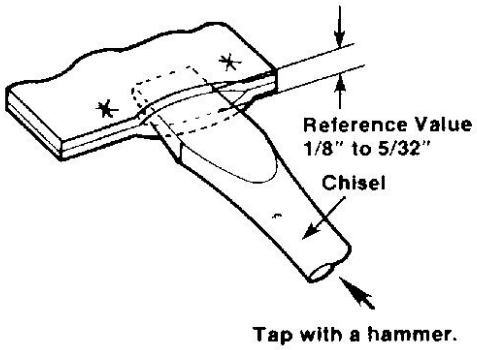

Figure 2.14 Method to perform the Chisel test (Courtesy of Nissan Motor Corporation).

Quoted as "destructive" testing, it means that the workpiece is fully destroyed after the tests. Besides chisel test, additional cost is incurred because the workpiece has to be destroyed during the test. Furthermore, it can only be done off-line and by sample (batch) checking. Therefore, the real-time, in-situ measurement and cost efficiency are difficult to achieve.

2.5.2 Non-Destructive Evaluation of Weld Quality

Non-destructive testing (NDT) is of vital important and because of the obvious demand from shop floor for quality assurance purpose. Some of them has been applied with varying degrees of success in RSW such as ultrasonic inspection used in the car industry.

But, many others are still in the primarily stage of development. These methods are summarized and discussed in detail as following:

(1) Ultrasonic Inspection [15] [16]

The ultrasonic inspection has been implemented in the present car industry due to its superior advantages to other NDT methods. Theoretically, a high frequency ultrasonic energy is generated by a probe and emitted through the material in the form of waves. When a crack or discontinuity is found along the wave path, some of this waveform energy is reflected back from this flaw. This reflected signal is then displayed as signal strength versus the signal traveling time. Based on the above information, the flaw location, size and shape can be obtained.

For this method, the deep penetration of ultrasonic waveform and single-sided probe assessment makes it very efficient in flaw detection. It also produces a high accuracy in determining flaw position and estimating the size. For car industry, it has been used as an off-line monitoring system for RSW. In fact, the defects of RSW are classified into 9 categories: (1) Good; (2) Stick weld; (3) Burned; (4) Small nugget; (5) Bad through; (6) Loose weld; (7) Heavy indent; (8) Shallow indent; (9) Gaspore (Courtesy of China Motor Corporation).

In practice, it is rare to see the real time ultrasonic inspection, which is installed in the production line due to its high cost and complex operation system. Therefore, extensive

training has to be provided for operators. Material with rough, irregular or curve surface is difficult to inspect because only flat surface is best accessible for ultrasound. Low sound transmission material such as cast iron is also difficult to apply this method.

(2) Dynamic Electrical Resistance Monitoring [9]-[11] [13] [17]

As mentioned earlier, the dynamic electrical resistance has been quantitatively studied recently because it is potentially used to monitor the weld quality based on real time measurement. The easy assessment and measurement of this method, and real time response are the advantages which makes it very suitable for shop floor application. Basically, the resistance can be calculated by measuring the voltage and welding current at the current peaks across the electrodes to avoid inductive noise [17] or adopting a numerical model with consideration of temperature, pressure and etc [13]. But, for the first method, the resistance is not time-varying because it is obtained as a single point only for every half cycle of current signal. Besides that, the accuracy of second method is in doubt although it can produce time-varying resistance signal. Therefore, none of the above methods can provide accurate judgment of weld quality.

(3) Dynamic Electrical Resistance Measured from Primary Circuit [18]

The measurement of dynamic resistance is mentioned in (2). However, engineers always face a problem in measuring the current because it can go as high as 10 kA for a spot weld. Alternatively, this current signal can be measured from the primary circuit and it is

much lower (less than 100A). But, the dynamic resistance obtained from this method is highly distorted due to the large inductive noise incurred by the welding transformer. Cho suggested that the secondary dynamic resistance is calculated by dividing the instantaneous voltage from current when the derivative of the current is zero. Thus, the secondary dynamic resistance can be converted from primary dynamic resistance without the inductive noise.

Similar to the method proposed by Wei Li [17], this method is approximate method also because only a data point is obtained for every half cycle of current signal. Therefore, it cannot provide an accurate and time-varying signal in this case.

(4) Electrode Displacement Monitoring Method [19]

The electrode displacement is one of the alternatives for quality monitoring. A high-speed video imaging system is used to measure the electrode displacement of the small scale resistance spot welding (SSRSW) process at real-time basis. Theoretically, the electrode displacement curve can be compromised of two identifiable segments. The high velocity segment of displacement curve is corresponding to solid-liquid phase transition in the weld nugget. On the other hand, the magnitude of this high velocity segment can be correlated to the weld nugget thickness. Therefore, it can provide the information about the formation of weld nugget.

For this method, it is only suitable for SSRSW because its accuracy is significantly affected by the vibration of welding machine in large scale resistance spot welding. As a result, further confirmation is needed for implementing this method.

(5) Thermal Expansion Displacement Monitoring Method [20]

This is an improved electrode displacement monitoring method, which can be used for either small or large scale RSW. Li *et al.* introduced a kind of precision laser displacement sensor and mounting jig to measure the electrode displacement. After the laser was calibrated and the measured signal was correlated with welding current, the weld quality could be obtained. Although this method can be done real-time and its accuracy is high due to precision measurement of laser sensor, the calibration and positioning of the sensor on the welding machine are very time consuming and subsequently jeopardize the production.

(6) Acoustic Emission Inspection [21]

Another potential in-situ and real-time monitoring method made use of sonic emission was suggested by Primoz Podrzaj *et al.*. The welding strength is correlated with the emitted acoustic signals at the vicinity of spot weld during welding process. Since the capturing of sound was done by a microphone near to the welding area, the noisy environment in production floor could affect the accuracy of this method significantly.

CHAPTER 3

INPUT ELECTRICAL IMPEDANCE OF RSW

In this chapter, the input impedance of a dynamic system is first introduced. How well this input impedance can be correlated with the RSW system and therefore the weld quality is also discussed. A case study based on good and bad welds will be reported for investigating the capability of input impedance as a quality monitoring signature.

3.1 Input Impedance of a Dynamic System

Fig. 3.1 shows a dynamic system with excitations and responses at its input port. Basically, the responses should only exist as a result of the excitations applied to the system. If the system properties are unchanged, the responses should change according to the variation of excitations. In other words, the dynamic behavior of such system can be described by the quotient of excitations and responses. Such definition can be used to describe different systems. For an example, the quotient of torque and angular velocity is known as mechanical impedance. In this thesis, the electrical input impedance (Z_{in}) which is defined as the quotient of input voltage and current, is the key factor to be investigated. Any change of this impedance should only reflect the change of the system properties.

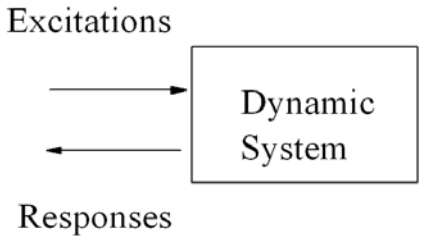

Figure 3.1 Dynamic system with its excitations and responses at input port.

3.2 Input Impedance of a Time-Variant System Operating at Single Frequency

For a linear time-invariant system, its system property is very often described by frequency response function. By using dynamic signal analysis via fast fourier transform (FFT), this FRF can be evaluated in frequency domain. The definition of FRF is shown in Eq. (3.1). As mentioned earlier, the input impedance of system is defined as the quotient of excitations and responses. In theory, both variables are function of frequency. Therefore, this impedance can be also expressed as shown in Eq. (3.1) but now the $H(i\omega)$ is input impedance, $Y(i\omega)$ is excitation and $X(i\omega)$ is response of the system.

$$H(i\omega) = \frac{Y(i\omega)}{X(i\omega)} \tag{3.1}$$

Where $H(i\omega)$ is frequency response function;

$Y(i\omega)$ is transfer function of output;

$X(i\omega)$ is transfer function of input;

However, there are some cases whereby the system operates at single frequency only. For an example, the running speed of an AC motor seldom changes under constant loading because it always operates at a fixed frequency of input power. Another example is resistance spot welding. Due to the frequency of input power to welding machine is fixed, it is considered as single frequency input. Therefore, the input impedance should vary with respect to the time at the particular frequency. The system with such behavior is known as time-variant system.

3.3 RSW System and Its Input Impedance

A basic RSW system and its equivalent electrical circuit are shown in Fig. 3.2. For the electrical circuit, it consists of resistance (*R*), inductance (*L*) and capacitance (*C*). When voltage is being applied, current will start to flow through the system. Obviously, the response (current) of the system is solely initiated by the excitation (voltage) at the input port of the RSW system. As a result, the input electrical impedance (Z_{in}) of the circuit is defined as the quotient of input voltage and current. With the description given above, the Z_{in} characterizes dynamic behavior of the RSW system. Any variation of Z_{in} indicates the changes of *R*, *L* or *C* during welding process. Their changes can be solely caused by the variations of the system properties such as thermo-mechanical behavior at the electrode to sheet interface and the faying surface. Furthermore, the RSW is considered as a time-variant system. It is because its Z_{in} is also known as single frequency signal due to the single frequency of input power. Therefore, the variations of Z_{in} shall reflect the variations of *R, L* and *C* in time domain.

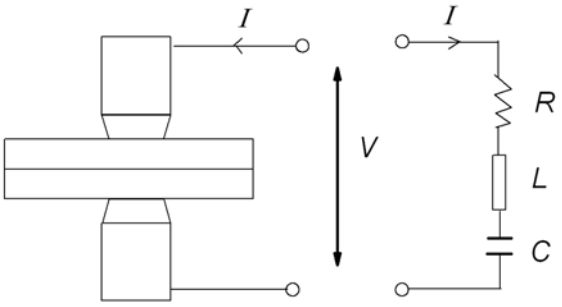

Figure 3.2 Equivalent *RLC* circuit.

In order to obtain the Z_{in}, the input voltage is divided by input current according to Equation (3.1) in time domain. Since both signals are AC signals, the direct division is impossible in this case. One way to solve this problem is to let both signals to be first converted into analytical signal by using Hilbert Transform method [22]. The analytical signal of a signal $X(t)$ is

$$\hat{X}(t) = X(t) + \frac{i}{\pi}\int \frac{X(t')}{t - t'} dt' \tag{3.2}$$

where the imaginary part is the Hilbert transform of the real-time signal. The input electrical impedance is obtained as

$$Z(t) = \frac{\hat{V}(t)}{\hat{I}(t)} = \frac{\left|\hat{V}(t)\right|}{\left|\hat{I}(t)\right|} e^{i[\varphi_1(t) - \varphi_2(t)]} = \left|Z(t)\right| e^{i\varphi(t)} \tag{3.3}$$

$$Z_{in} = Z_r + i\omega Z_x \tag{3.4}$$

where $\hat{V}(t)$ and $\hat{I}(t)$ are the analytical signals of voltage and current respectively, $|Z(t)|$ is the amplitude of input electrical impedance and the $\varphi(t)$ is the phase between the voltage and current signal. In Equation (3.4), it reveals that the impedance can be expressed in complex form. The real part (Z_r) and imaginary part (Z_x) of Z_{in} actually equals to the resistance and reactance of the equivalent circuit. Basically, the real part represents the energy being removed from the system in form of thermal heating. Therefore, work is done by melting the metal sheets at faying interface and joining them together. For *C* and *L* in the system, no work is done by the imaginary part because the energy is usually stored and then released. With the preliminary evaluation about the Z_{in}, more detail about its relationship with physical change of RSW will be discussed in the following chapters.

Fig. 3.3 shows the experimental set-up for Z_{in} acquisition. A 50 Hz single phase AC, 75 KVA rated power pedestal type welding machine with water cooling system for the electrodes was used. Besides that, an aluminum jig was made and mounted in between 2 electrodes to clamp and hold the workpieces (see Fig. 3.4). From Fig. 3.5, it can be seen that the jig consists of a nylon plate to support the workpieces and more importantly to prevent current shunt problem. Furthermore, an angular adjustment device with 1º resolution was designed to adjust the inclined angle of workpieces up to 15º. The screw at the 4 corners and 1 long screw are used for the angular adjustment. Additionally, a quick locking device was designed also in order to rule out the problems of having poor fit-up, edge weld and axial misalignment during welding process.

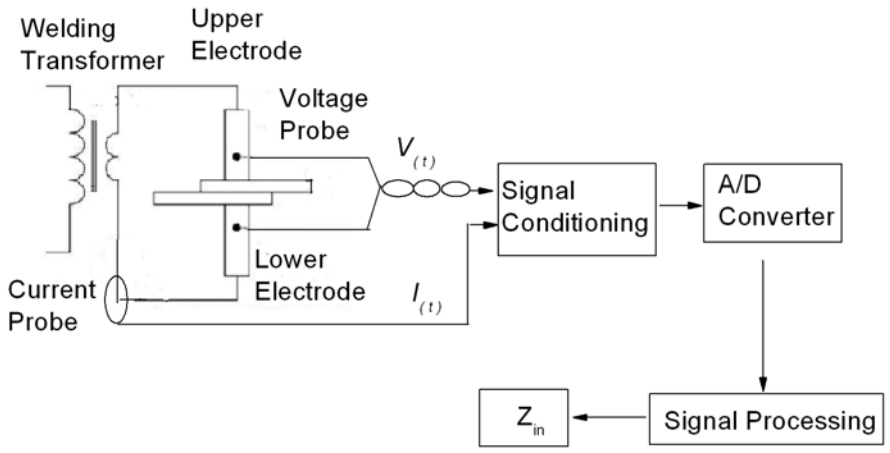

Figure 3.3 Experimental set-up for signal acquisition.

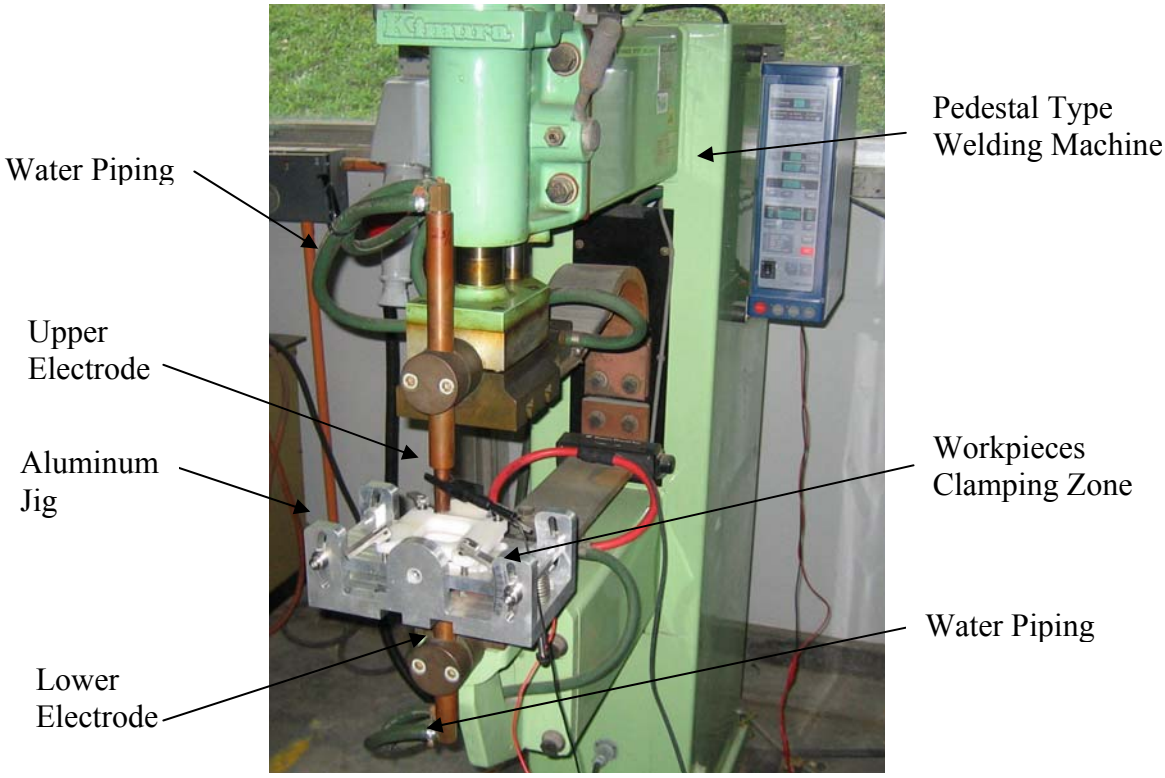

Figure 3.4 Aluminum jig mounted in between 2 electrodes.

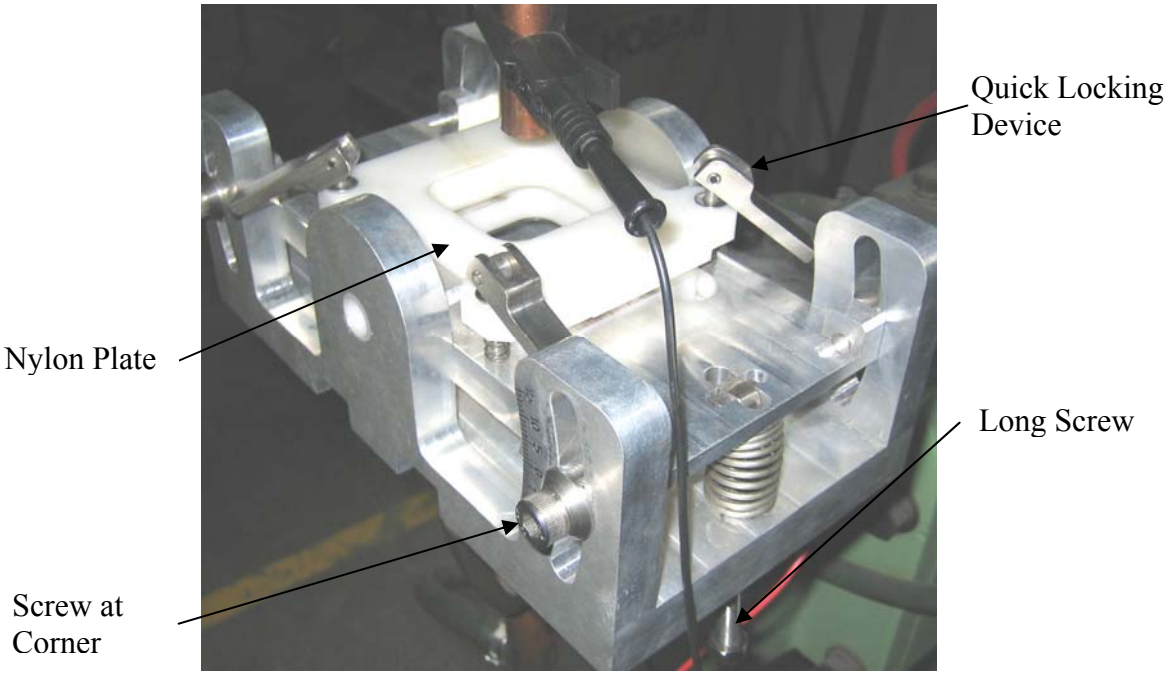

Figure 3.5 Nylon plate on top of Aluminum jig.

For signal acquisition, a toroidal coil type current probe and a simple BNC cable with crocodile clips end were used to measure the welding current and voltage. Since the measured signals are AC waveform, the polarity of the voltage has to be put in phase with current to prevent 180º phase delayed. Both analog signals were measured simultaneously once the current started to flow. For signal conditioning, a 2 channel low pass filter with 80Hz cut-off frequency was used for anti-aliasing purpose during the analog signals sampling. After the analog signal filtering, 12-bits A/D Converters with 2 channel inputs were used to sample the signals at 2.5 kHz. During signal processing, a digital, 6^{th} order low pass filter was utilized in the program to filter out the sub-harmonics components before calculating the Z_{in}. The whole process was done by using Matlab™ program.

In order to obtain accurate and consistent result, there are 2 precautions to be considered carefully. In mechanical measurement, a commonly seen problem is known as signal leakage [23]. It is because the original signal cannot be completely reconstructed from its digital form when the total sample period is not coincident with an integer multiple of the fundamental period of original signal. In RSW, this problem is mainly caused by the welding time is always fixed at certain cycles. In other words, the signal record length has to be coincident with the total welding time or else signal leakage problem will occur.

Another problem about signal measurement in RSW is the triggering of signal acquisition. As external signal triggering mode is used, the signal acquisition is triggered randomly by current signal. Therefore, bi-polar (windows) triggering mode has to be used in order to eliminate the tendency of signal missing for the first half cycle. Otherwise, the first peak in Z_r will be missing from its waveform.

3.4 A Case Study of RSW with Impedance Waveforms

For this research work, low carbon steel with 2 different thicknesses, 1.0mm and 1.2mm were simply used since M. Zhou [24] has found out that only the width of workpiece affected the accuracy of shear testing result. Therefore, the size of workpiece (as shown in Fig. 3.6) was carefully selected and dimensioned by using laser cutting to provide good surface flatness and edge finishing. This is important because any poor fit-up of the workpiece, as mentioned by Wei Li *et al.* [25], can be prevented. Furthermore, the workpiece were submerged into Ethanol for 15 minutes and rinsed before they were used

for RSW. All the operating parameters were set and the welding strength obtained for each weld was judged according to the R.W.M.A. Standard, Class A [Appendix A].

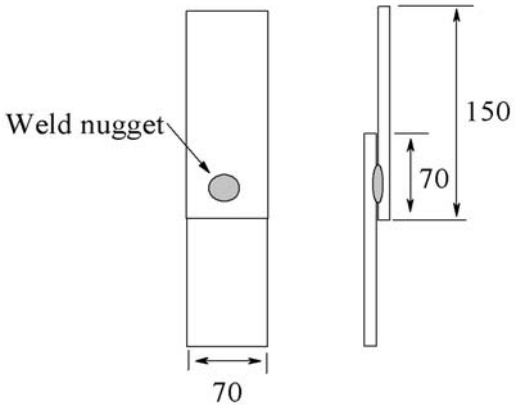

Figure 3.6 Workpiece dimensions in mm.

Fig. 3.7 and 3.8 showed the Z_r and Z_x of the Z_{in} for a spot weld. The waveform of the real part is comparable to the dynamic resistance method discussed in Chapter 2. It was observed that the waveform of Z_r was a continuous resistance curve varying with respect to welding time. In fact, the feature points as shown in Fig. 3.7 were important, which accurately reflected the physical changes of RSW system. The alpha peak represented the time when the temperature was increasing until the asperity surface broken down at the faying interface. It reduced dramatically to the throat and started to increase gradually due to the higher temperature and growth of weld nugget. Therefore, the beta peak was suspected to be related with the weld nugget formation. An in-depth study about the characteristic of Z_r waveform will be presented in later chapters.

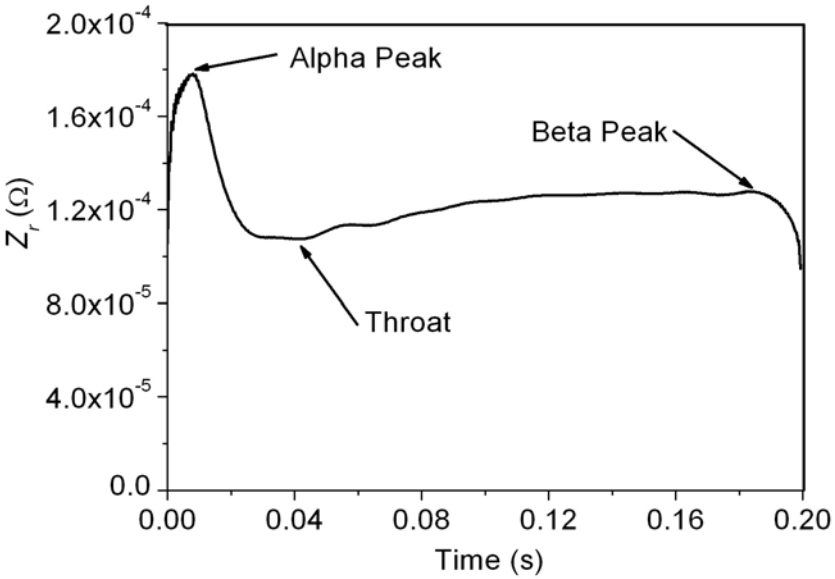

Figure 3.7 Real part (Z_r) of Z_{in}.

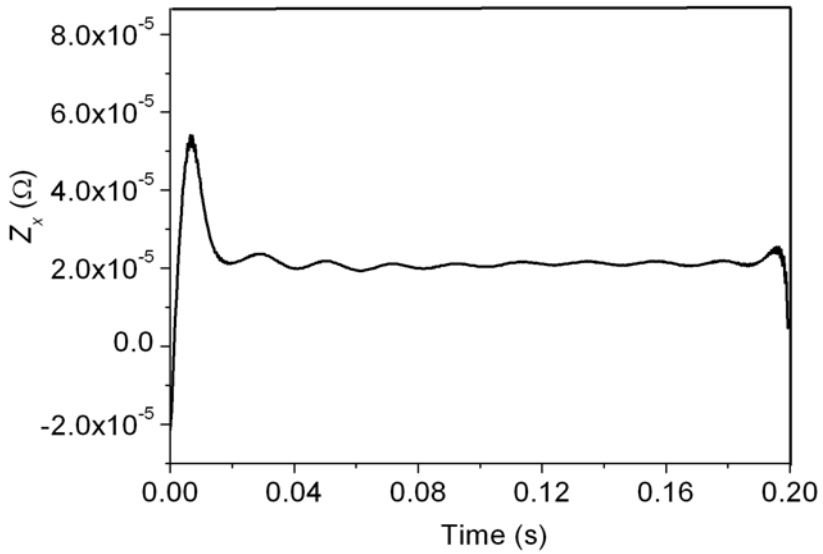

Figure 3.8 Imaginary part (Z_x) of Z_{in}.

3.5 Weld Quality and Impedance Waveforms

Since the Z_r could be correlated with the physical change of RSW closely, a further investigation was carried out to confirm the capability of Z_{in}. Fig. 3.9 demonstrated the Z_r obtained from 10 spot welds based on welding current variation. By performing tensile-shear testing, the welding strengths indicated that half of them were good welds and the rest were bad welds [Appendix F]. The comparison between these waveforms provided some clues for feature points selection. Basically, the feature points at the throat and beta peak were selected because they showed a significant difference between good and bad welds. Other feature points could be selected based on later discussion in the following chapter.

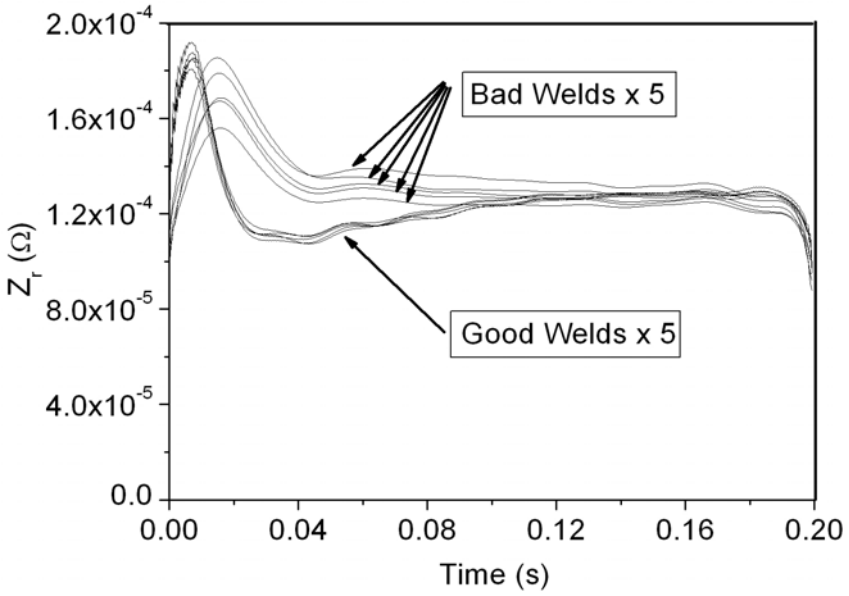

Figure 3.9 Real part of Z_{in} based on welding current variation.

In previous research work, Ling *et al* [26] has proved that the input impedance is an inherent property of a linear dynamic system and does not vary due to the variations of the system input. When monitoring a manufacturing process, the variations of the manufacturing conditions are reflected by the changes of the input impedance of the manufacturing system. The applications of this concept in ultrasonic welding, micro drilling, and wire bonding [27]-[29] have confirmed the convenience and accuracy of the input impedance of a manufacturing system as a monitoring signature. In the following chapter, the proposed method will be further investigated in order to confirm its capability in developing a monitoring system for RSW.

CHAPTER 4

AN AUTOMATED WELD QUALITY MONITORING SYSTEM BASED ON Z_r WAVEFORM

An automated weld quality monitoring system is proposed in this chapter using Z_r waveform as monitoring signature. By introducing a pattern recognition and classification system equipped with an Artificial Neural Network (ANN), the proposed system can be achieved. Furthermore, a conceptual design of the proposed system will be presented at the end of chapter in order to confirm its capability as a desired quality monitoring system.

4.1 Pattern Recognition and Classification by Artificial Neural Network

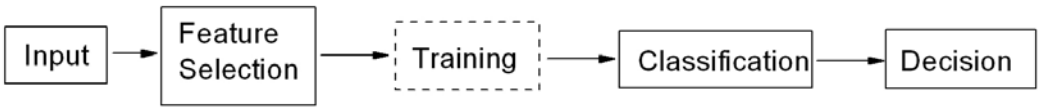

Figure 4.1 General pattern recognition and classification system.

A general pattern recognition and classification system is shown in Fig. 4.1. Firstly, the raw data is obtained by the data acquisition system. It involves analog signals measured

by sensor or probe, signal conditioning and signal processing so that the signals are properly condensed and in a form ready for computer processing.

For feature selection, the process data is further reduced into information which is directly related to the monitoring purpose. In practice, the size of process data, in terms of discrete data points, is usually very large. For an example, the data points for Z_{in} based on 10k Hz sampling rate, 0.2s welding time, is 10024 data points per either Z_r or Z_x waveform. In order to save computational processing time and memory space, the concept of feature selection is used. Basically, the Z_{in} can be represented by a much smaller group of data points which are extracted from its waveform. These points are then known as feature points of the Z_{in}. If the number of feature points can be kept as low as possible, the overall performance can be improved significantly. Therefore, the feature selection plays a major role in the system and will be discussed later in detail.

In the next stage, 2 major processes are introduced. Initially, a suitable algorithm such as fuzzy logic or ANN has to be selected. Before it is ready for pattern classification, a proper learning process has to be completed by using a set of known input and output values in pairs for the system to learn the pattern of Z_{in} waveform. This learning process can be very fast if a proper combination of feature points and algorithm are used. Therefore, iterative step of feature selection associated with different algorithm construction is usually involved in this stage. After learning process is done, the system can automatically perform the pattern classification by feeding in the feature points. In this thesis, the ANN is used to solve for the weld quality monitoring problem.

4.2 Feature Selection of Z_r Waveform

As mentioned above, the feature selection is an important process in the system because a group of well selected feature points can significantly reduce the number of data points and hence improve the efficiency and accuracy of the system. There are plenty of feature selection methods available such as Principal Components Analysis (PCA) [30], Factor Analysis (FA) and Multivariate Analysis of Variance (MANOVA) [31]. However, none of them is used in this thesis because they are mainly developed for large data size processing such as image pattern recognition and etc. For Z_{in} waveform pattern classification, these methods are not necessary because the feature points of Z_{in} are selected based on physical understanding of RSW.

In Fig. 3.9, it revealed that the Z_r waveform can distinguish the good and bad welds. Therefore, it is used as the monitoring signature without considering Z_x first to examine its capability of pattern classification. By comparing the good and bad welds based on the Z_r waveform only, 6 feature points were selected (see Fig. 4.2). The (t_2, r_2) and (t_3, r_3) represents the time and its corresponding Z_r values where the trough and beta peak are located. Based on the preliminary discussion in Chapter 3, the 4 features points are selected because they are related closely to weld nugget growth. Furthermore, the r_1 at 0.02s represents the beginning of welding process which reflects the asperity surface broken down at faying interface during the initial stage. Selecting r_1 can further reduce the feature points to one only by fixing the time at 0.02s. Similarly, the r_4 at 0.2s are

selected to represent the end of welding process which is related to the weld expulsion (will be discussed in next chapter). Eventually, these feature points are grouped into a feature space and then used for ANN learning and classification purposes.

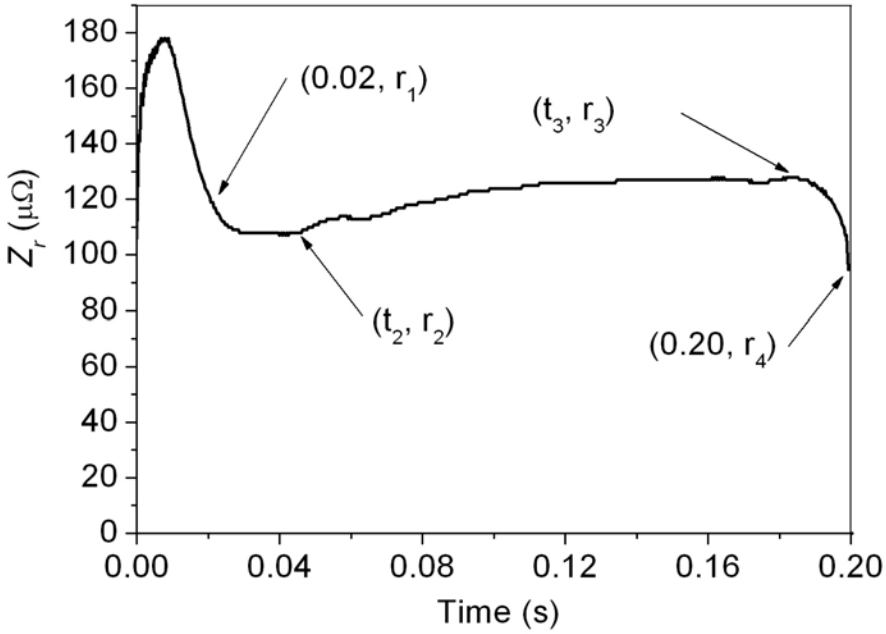

Figure 4.2 Feature points along the Z_r waveform.

4.3 Automation of Weld Quality Judgment

The ANN is used for pattern recognition and classification of Z_r waveform in this thesis because it is good for solving the non-linear relationship between the feature space and weld quality [32]. There are number of different neural network algorithms for ANN use. However, the Feed Forward Network with Back Propagation training algorithm was used because it could perform "self-learning", which could improve the accuracy of classification significantly. Basically, a 3 layer network structure was constructed. The

first layer is referred as input layer for the input feature space and followed by the hidden layer. The decision made by the neural network was then reflected at the output layer. For the hidden layer, "Sigmoid Transfer Function" was considered and "Purelin Transfer Function" was used in the output layer. The "Levenberg-Marquardt" [33] training technique was adopted for the ANN training because it appeared to be the fastest method for training the ANN. Matlab™ Neural Network Toolbox was used to solve the above problem.

The ANN was only able to deliver the desired output after proper training via a set of training data has been done. The capability of the trained ANN for weld quality classification was then confirmed by using another set of testing data. These 2 set of data were actually in matrixes formed by the feature space. Furthermore, 84 spot welds (using 1.2mm thickness low carbon steel) were done based on different process conditions to obtain the data sets as shown in Table 4.1. The good and bad welds were found by the tensile-shear testing. For the hidden layer, the number of neurons can only be set based on the accuracy and efficiency of ANN. During the training process, those weighing function (iw{1,1}, iw{2,1}) and bias function (b{1}, b{2}) are computed iteratively so that the error of ANN output converges to the training goal with known outputs in target matrix (see Fig. 4.3).

Table 4.1 Number of recorded data for training and testing.

	Number of training data	Number of testing data
Good welds	36	6
Bad welds	36	6

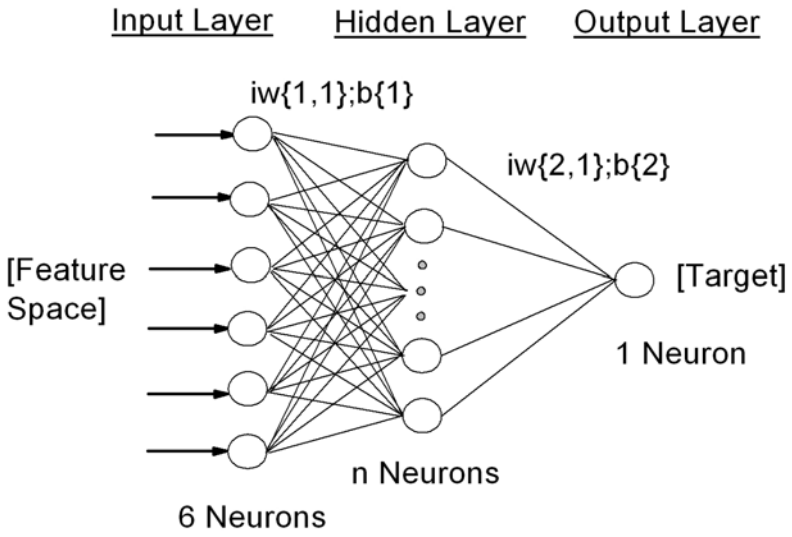

Figure 4.3 Neural network structure for the ANN.

As shown in Fig. 4.3, a 6 x 72 matrix including good and bad welds training data was fed into the 6 input nodes of ANN. There was only 1 output node showing '+1' or '-1'. As welding strength indicator, the "+1" denotes as good welding strength and vice versa. For the number of neurons in hidden layer, 5 nodes were eventually used as compared with other trials because it could achieve the fastest training speed (less than 1000 epochs) for a few seconds of computational time with the training error (training goal) set at 10^{-10}.

The trained ANN was then tested by using the 12 testing data sets. The testing results are plotted against the target value as shown in Fig. 4.4. It was observed that the ANN outputs matched perfectly with the target value for good welds. Out of 6 bad welds, 2 ANN outputs were deviated from -1 but remained negative while the outputs for good welds were totally exact as the target value. If a threshold at "0.0" line is considered and taking the sign of output neuron as the quality indicator as normally done, the accuracy of the created classifier is 100%.

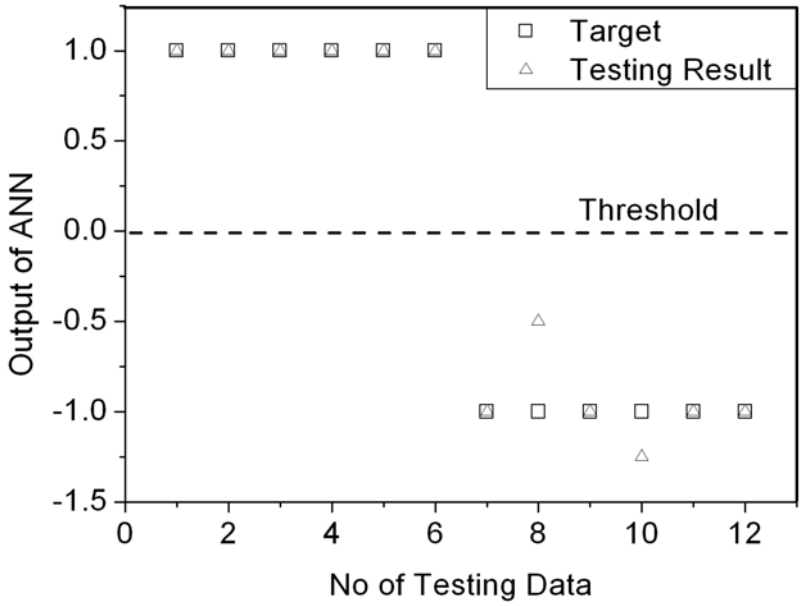

Figure 4.4 Result of ANN prediction.

4.4 A Conceptual Design of Automatic Weld Quality Monitoring System

The results presented in this chapter showing that the Z_r waveform is a very good signature to evaluate the quality of RSW. It is a time-variant waveform, which its feature

points can be closely correlated with the complicated physical change of the welding process and such change will be directly reflected by its weld quality in terms of welding strength. Therefore, an automatic, real-time and on-line quality monitoring system can be developed for RSW.

For the implementation of this method, it can be done by tapping the voltage and current probes to the electrodes so that it does not jeopardize the normal operations. As mentioned earlier, the whole monitoring system can be fully automated by employing an ANN. After proper training is done to correlate the feature space of Z_r waveform with the welding strength, the ANN is able to evaluate the welding strength by taking in the feature space from the waveform and output the weld quality of a weld almost instantly.

The hardware implementation of the monitoring system is shown in Fig. 4.5. Basically, there are 4 major components: (1) Sensing elements; (2) Signal conditioning; (3) Signal processing and storage; (4) Output elements. The input voltage and current signals have to be sensed by using the probes. For the current probe, proper input and output range of probe has to be used. Once the welding process starts, these 2 signals are acquired by the A/D converters via an anti-aliasing analog filter. After the analogue signals are converted to digital signals, the computation of Z_{in}, Z_r feature extraction and the ANN prediction will be performed by a micro-processor. Furthermore, all the processed data will be saved in a memory storage device for further analysis and reporting purpose. Finally, the prediction of ANN will be output by a horn and LED light to alert the operators for any detected bad weld. Fig. 4.6 shows how does the system is realized by using an embedded

signals acquisition and processing system. The LCD display serves as an input and output device for the system so that the operator can select proper task for different applications.

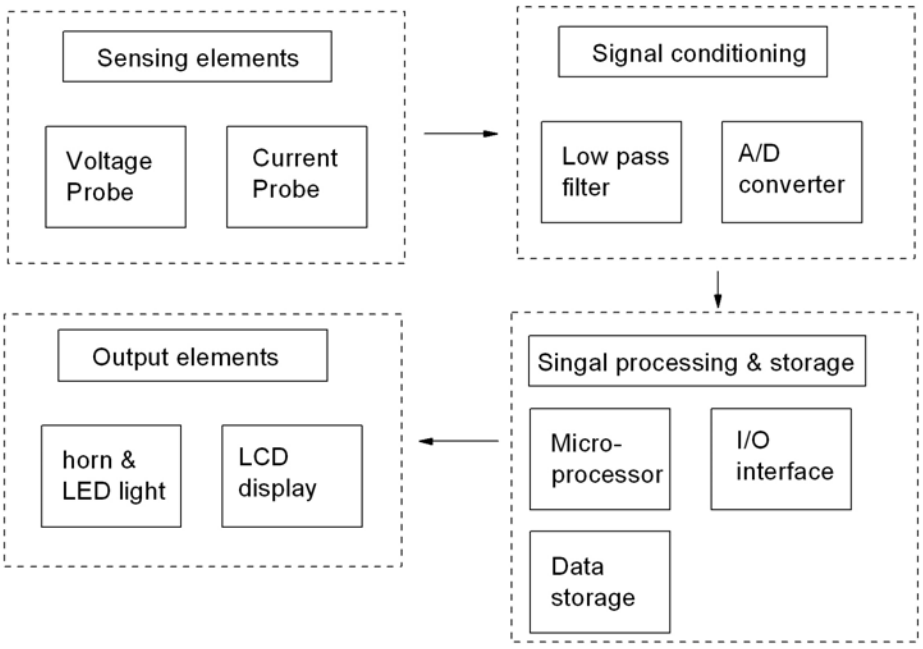

Figure 4.5 Hardware of the monitoring device.

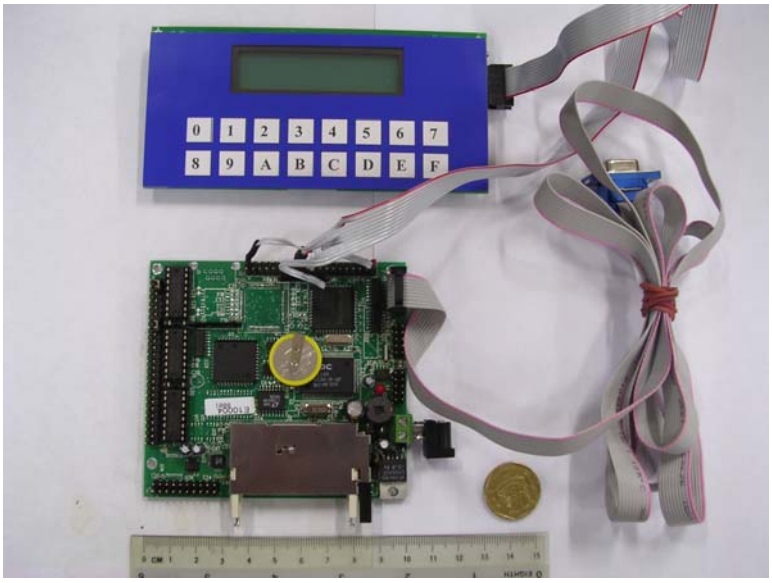

Figure 4.6 Embedded micro-processor system with LCD display.

In order to complete the conceptual design, the basic data processing flowcharts are also provided in Appendix E. There are 3 stages for the data processing flowcharts and each stage assists the software development for the respective task as mentioned above. By following the conceptual design presented above, a real-time, accurate, on-line and automatic weld quality monitoring device can be achieved.

CHAPTER 5

WELDING OPERATING PARAMETERS AND INPUT IMPEDANCE

The operating parameters and process conditions can be volatile during actual production situation. Fluctuation of pressure, variation of welding current, degradation of electrode and etc are usually unavoidable due to the harsh working environment. In Chapter 4, the welding current was manipulated to create sufficient data sets for ANN training and verification. However, the closed relationship between the Z_r waveform with those major operating parameters and process conditions has not been identified yet. Therefore, the problems with angled weld for abnormal process conditions; pressure, welding current and electrode are discussed separately and the experiments are carried out to evaluate their effects on Z_r waveforms. Summary of their influences and the correlations between the welding strength and the features of Z_r are presented at the end of this chapter. For the experiments, all the spot welds were made by 1.2mm thickness low carbon steel sheets with standard workpiece preparation procedure as mentioned in Chapter 3 in order to guarantee repeatable results. Furthermore, only 5 spot welds with their Z_r waveforms for those mentioned except electrode will be presented in this thesis.

5.1 Angled Weld

In many production occasions, either using hand-held welders or robots, the RSW is done on metal sheets positioned with fixtures. The inclined angle (Φ) between the electrodes and metal sheets could deviate from the assumed zero degree and form angles randomly in a range from spot to spot (see Fig. 5.1). Including others abnormal process conditions such as poor fit-up, edge weld and etc, Wei Li *et al.* [25] has reported that the mentioned abnormal process conditions could cause large variation in the weld quality. In fact, some of them were reported to be able to enlarge the weld nugget dimension but they led to a less robust welding process.

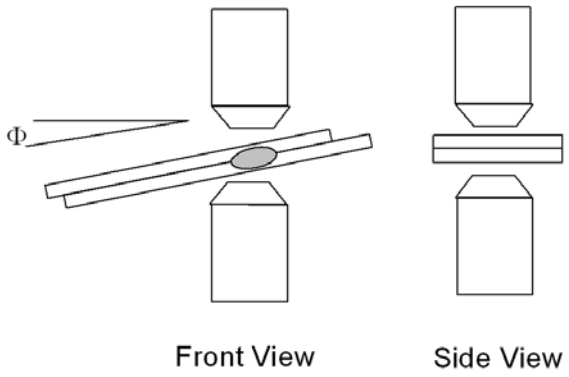

Figure 5.1 Angled weld with the inclined angle, Φ.

5.1.1 Evaluation of the Effects of Angled Weld on Z_r Waveform

As shown in Fig. 5.2, the aluminum jig mounted onto the platform of the welding machine was equipped with variable angle adjustment capability. The inclined angle can

be varied from 0º to 15º depending on the experiment. In order to evaluate the effects of angled weld on the Z_r waveform, 5 spot welds with 0º, 3º, 6º, 9º and 12º angled weld were shown in Fig. 5.3. For 0º, 3º and 6º angled welds, the waveforms showed a consistent pattern without much observable deviations. However, the waveforms with larger inclined angle were observed to have higher value before 0.08s welding time. Around 0.12s, all the Z_r rose to about 120μΩ. For the 12º angled weld, a sudden drop of Z_r was observed and defined according to the shape of waveform, which the Z_r plumped down sharply near to the end of welding process. This sudden drop was suspected to be caused by the expulsion of weld because the visual observation reflected this phenomenon during the welding process.

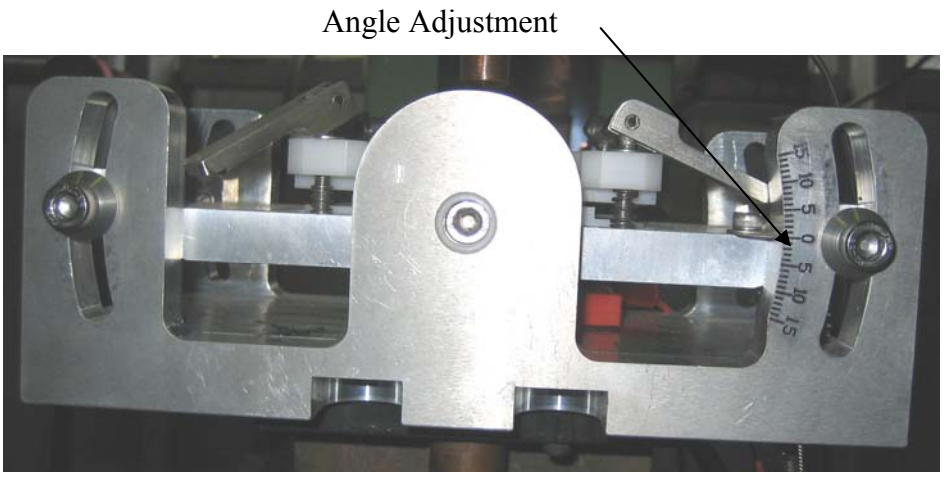

Figure 5.2 Aluminum jig with inclined angle adjustment.

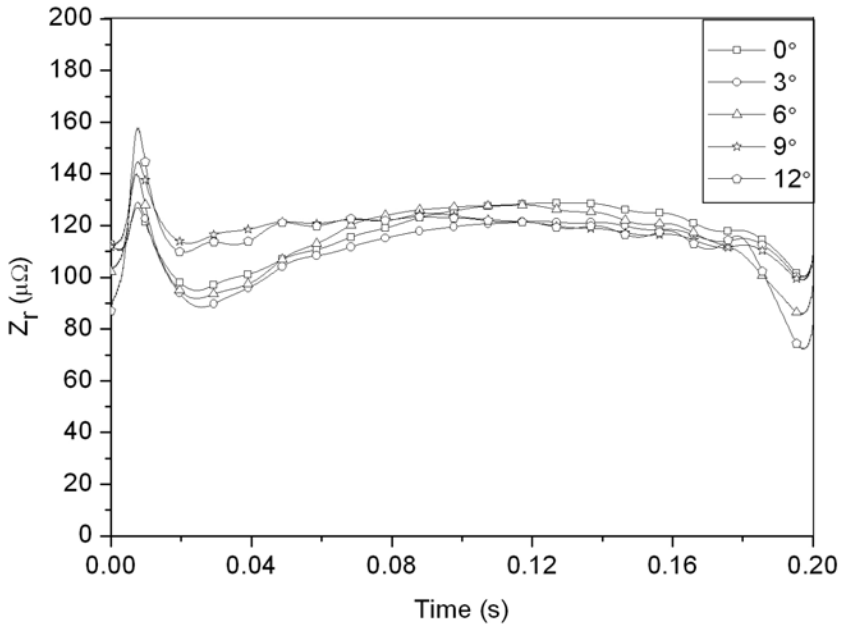

Figure 5.3 Z_r waveforms based on different inclined angle.

Based on the above observations, the deviations of Z_r near to the beginning and the end of welding process can be caused by the pressure applied on the contact interfaces. For truncated type electrode with flat tip surface, the full contact of electrodes with the surface of workpieces is made immediately if no inclined angle is found. Due to the direct and simple compression of electrodes, this intimate contact only requires minimum plastic deformation of workpieces under a constant pressure. However, it can be difficult for the electrodes to compress under the same pressure when the workpieces are tilted. The contact of electrode with the surface of tilted workpiece actually begins from the edge of electrode tip surface. If the electrodes compress further with increasing pressure, it provides necessity for the material to deform more so that the full and intimate contact condition can be achieved. In other words, additional pressure is required in order to have the same effect of compression for larger angled weld. Since the pressure is not changed

throughout the experiments, higher Z_r is obtained near to the beginning of weld as a result of low pressure. Furthermore, this is also confirmed by the occurrence of weld expulsion for 12º angled weld, which is often caused by the insufficient pressure.

For the weld expulsion causing sudden drop of Z_r, the reason can be found from Equation (2.2). For instance, the Z_r, or resistances of the RSW system, *l* refers to the total thickness of a lap-joint weld and *A* is the weld nugget dimension (welded area). According to Wong [34], he reported that the L was reduced for large angle welds due to the mass loss of the molten metal, which was ejected from the fusion region. Therefore, the Z_r drops rapidly to a lower value with constant ρ and A.

5.2 Pressure

Pressure, also known as electrode force, is one of the important operating parameters that affect the weld quality. In actual production occasion, the pressure supplied to the welding machines is difficult to control due to the fluctuation of the main pressure supply. Therefore, the weld quality of RSW suffers very often from the fluctuation of pressure because the operators are usually unaware about the change of pressure.

5.2.1 Evaluation of the Effects of Pressure on Z_r Waveform

Pressure was varied from 140% to 60% of RWMA CLASS A Standard in order to evaluate the effects of pressure change on the Z_r waveforms and they were presented in

Fig. 5.4. By comparing with the 100% pressure (2.7 kN) weld, it found that both lower and higher pressure welds were associated with a higher Z_r before 0.08s but the latter has the highest Z_r. Continuously, all the beta peak rose to about 120 μΩ but for higher pressure welds, it took place earlier around 0.08s. Near to the end of welding, the sudden drop of Z_r was observed with the occurrence of weld expulsion for lower pressure welds.

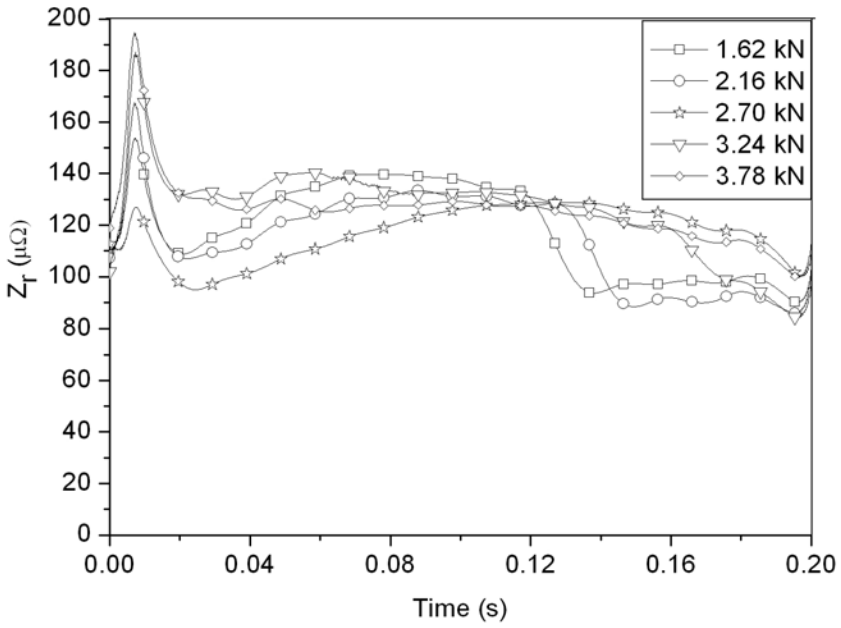

Figure 5.4 Z_r waveforms based on different pressure.

According to the literature study in Chapter 2, lower pressure will cause higher contact resistance. This is successfully reflected by the result shown in Fig. 5.3 and 5.4, which higher Z_r is obtained for 60% and 80% pressure welds as compared with the 100% pressure weld. However, the Z_r for 120% and 140% pressure welds are observed to be the highest. This finding is surprisingly contradicting with those reports because the resistance should be lowered due to the increase of contact area at faying interface,

shortened electrical path and higher heat conductive rate. In order to confirm this finding, the physical change of material shall be examined. As mentioned earlier, the resistance of RSW, or the Z_r of impedance, actually consists of bulk and contact resistance. For higher pressure welds, the contact resistance has to decrease according to the reasons reported in literature [4]. However, the bulk resistance is different because it increases when the temperature of material is increasing. According to the phase diagram of a mechanical system, the temperature of material shall be higher when the applied pressure is increased. Therefore, the temperature of material shall be higher for increasing pressure and cause the resistivity of material to be higher, which eventually results in a higher bulk resistance. Subsequently, the contribution of this bulk resistance causes the Z_r to be higher.

Compared with the angled welds, the occurrence time of expulsion is also different. The weld expulsion happens around 0.12s, which was earlier by 0.05s as compared with the angled weld. This can be due to the effect of lower pressure itself is more direct and significant. The more serious weld expulsions are also observed in the case of lower pressure welds.

5.3 Welding Current

Based on Joule's Law, the formation of weld nugget driven by heat generation is much related to the welding current. A lot of experimental work also reported that the poor weld nugget resulting into weak welding strength was mainly due to insufficient amount

of current flow during the welding process even though it has been set before weld. For industrial practice, ensuring the correct amount of current flow throughout the welding process is the key activity of weld quality assurance. Therefore, a constant current feedback system is normally used in the welding machines in order to control the current within the specification. However, this feedback system does not guarantee the amount of current is completely used for weld nugget formation because it can only control the current flow at the input port of welding machine. The current shunting at the adjacent contact point or edge weld actually diverts some of the current out from the welded area, which is undetectable by the feedback system.

5.3.1 Evaluation of the Effects of Welding Current on Z_r Waveform

5 spot welds with different welding current were presented in order to investigate the effects of current on the Z_r waveform. The welds were made starting from the standard welding current at 9.8 kA and then reduced to 9.0, 8.0, 7.0 and lastly 6.0 kA.

As shown in Fig. 5.5, the variations of Z_r waveforms showed a good correlation with the current change. According to the Ohm's Law ($R = \frac{V}{I}$), the resistance is inversely proportional to the current. With very little change of voltage, the resistance increases mainly due to the decrease of current. This was demonstrated by the Z_r waveforms for different welding currents. When the welding current was gradually decreasing from 9.8 kA to 6 kA, the Z_r increased by following the Ohm's Law, but the increase was not linearly dependent on the change of welding current. This could be due to the RSW is an

indeed complicated system, which is inaccurately described by using simple theory like Ohm's Law. From a different angle of view, the Z_r is able to reflect the behavior of RSW system accordingly.

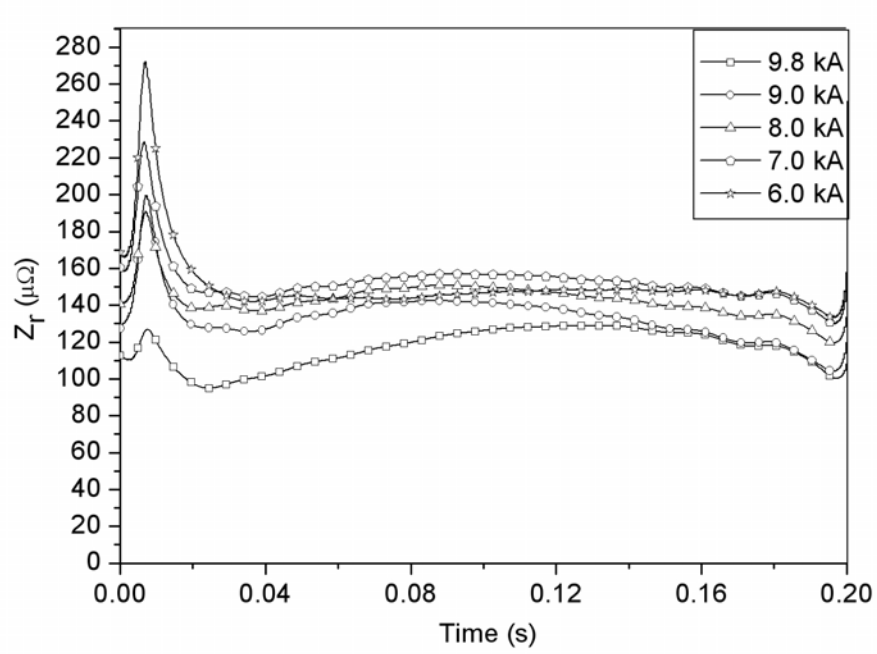

Figure 5.5 Z_r waveforms based on current variation.

Based on the results shown, the beta peak is potentially a good indicator for weld nugget formation. It is because the numerical difference of Z_r between beta peak and throat could be correlated with the weld nugget growth. For an example, by taking the throat and beta peak as 90 μΩ and 120 μΩ for 9.8 kA weld based on Fig. 5.5, the difference of Z_r is therefore 30 μΩ. However, this difference has been gradually reduced to 10 μΩ for 7.0 kA weld and lastly 0 μΩ for 6.0 kA weld, which no weld nugget is actually formed after the welding process.

5.4 Electrode

The copper alloy made electrode is used as the only consumable part for RSW. The life span of electrode can be from few hundreds to thousands of welds depending on the process conditions such as material to be welded, cleanliness of surface and other operating parameters. Basically, the deterioration of electrode can be categorized like surface pitting, surface enlargement and uneven surface flatness after continuous use in production. When the electrode is found to be deteriorated, it is then changed by a new electrode with flat and smooth surface.

5.4.1 Evaluation of the Effects of Tip Surface of Electrode on Z_r Waveform

2 electrodes with poor tip surface condition were arbitrary created in order to simulate the uneven surface problem. From Fig. 5.6, a 1.5mm grove at the center and 2.0mm width of side chipped off were made for the spot weld. The corresponding Z_r waveforms were then compared with the one made by normal electrode to examine its effects on Z_r waveform.

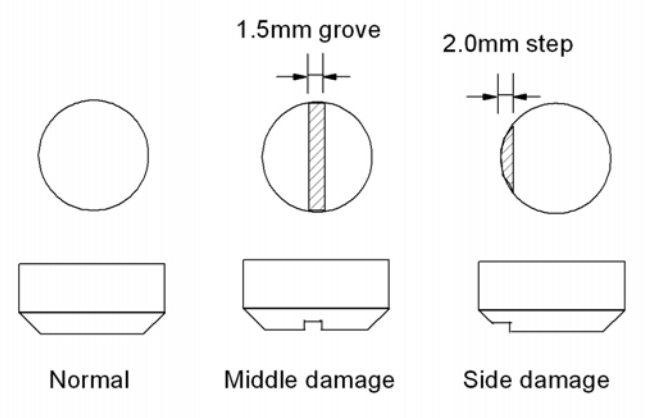

Figure 5.6 Tip surface conditions of electrode.

Compared with the normal weld, the middle and side damage welds showed a significant difference. In Fig. 5.7, it was observed that the sudden drop of Z_r happened 2 times for side damage weld. Firstly, the sudden drop of Z_r started around 0.08s but it rapidly increased again around 0.16s. Furthermore, its Z_r value was also much higher than the middle damage and normal weld throughout the welding process. For middle damage weld, the Z_r was higher than normal weld before 0.08s but their beta peaks were the same around 0.12s. The sudden drop of Z_r was also observed for middle damage weld around 0.15s. Similar to the result of pressure and angled welds, this sudden drop of Z_r was associated with weld expulsions.

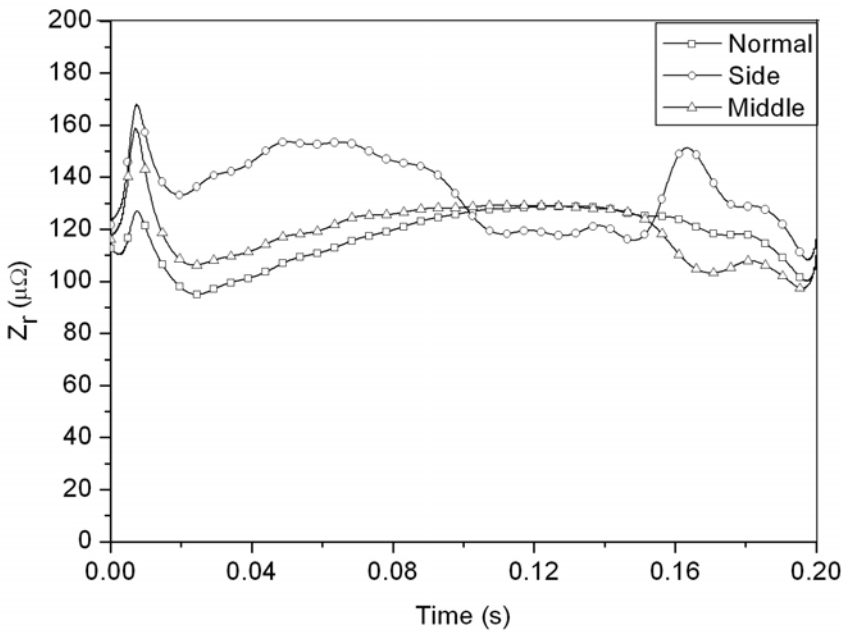

Figure 5.7 Z_r waveforms based on different tip surface conditions of electrode.

The observation of side damage weld shows that a very severe weld expulsion happened during the welding process. The expulsion is so bad that a small through hole is formed at the location of side damage as a result of molten metal ejection. Near to the end of welding, only a small weld nugget is formed under the welded area where the tip surface is flat. In fact, this phenomenon was reflected clearly by the Z_r waveform shown in Fig. 5.7. The big drop of Z_r from 0.08s to 0.16s implied that the electrical path length is shortened due to the massive loss of molten metal. Furthermore, its waveform was also much higher than normal and middle damage weld throughout the welding process. It is believed to be caused by higher pressure at the flat surface area due to the reduction of total contact area. For the middle damage weld, the Z_r is higher than the normal weld before 0.08s. It is actually caused by a smaller contact area with the presence of center grove.

5.5 Discussions of the Z_r Waveform Correlations

Based on the presented results, the effects of operating parameters and process conditions can be concluded as a result of the change of pressure and welding current. The variation of pressure itself, pressure reduction due to angled weld and degradation of tip surface of electrode cause the Z_r to deviate. Either low or high pressure will cause a higher value of Z_r before 0.08s but the effect of higher pressure is the most significant. For low pressure, the Z_r waveform normally encounters a sudden drop of Z_r near to the end of welding due to the occurrence of weld expulsion.

The change of welding current is also reflected by the deviation of Z_r waveform. By following the Ohm's Law, the Z_r value shall increase when the current decreases and vice versa. In other words, the level of Z_r actually indicates the amount of current that is used for heat generation and subsequently the formation of weld nugget. Furthermore, the weld nugget growth is proved to be related with the difference of Z_r between the throat and beta peak. Therefore, this feature can be used to determine the welding strength of RSW. The smaller the difference is, the weaker the welding strength will be.

The sudden drop of Z_r can be an important indicator for the occurrence of expulsion. Based on the results shown in this chapter, the time of occurrence can be used to indicate the seriousness of expulsion. The visual observations show that the serious case of expulsion happens around 0.08s for side damage weld; the moderate case of expulsion is

considered for low pressure weld and it takes place around 0.12s (see Fig. 5.4); the light expulsion is observed for angled weld and the time of occurrence is around 0.16s (see Fig. 5.3). Therefore, the seriousness of expulsion can be simply obtained by knowing the time of occurrence for sudden drop of Z_r.

The welding strength for all the spot welds is tested also in order to correlate the weld quality with the features of Z_r waveform. According to RWMA Class A Standard, the welding strength is good for angled welds and pressure welds. However, bad welding strength is tested for welding current below 8.0 kA and side damage weld. Therefore, the combination of alpha peak and throat can be used to indicate the pressure drop; the combination of throat and beta peak can represent the weld nugget growth and hence it's welding strength; the sudden drop of Z_r shows the occurrence and seriousness of weld expulsion; and lastly the combination of alpha peak, throat and beta peak are used for welding current reduction. The conclusion drawn in this chapter will greatly improve the feature selection for the automated system, which is introduced in Chapter 4.

CHAPTER 6

MICROSTRUCTURES OF WELDS AND Z_r

The input impedance has been discussed in the previous chapters for it's usefulness in real time quality monitoring capability and the good correlation between the features of Z_r with the operating parameters and process condition. However, there is still room for improvement to enhance the knowledge about the Z_r waveforms since it has such a good correlation with those important factors. Therefore, the Z_r is firstly verified by the physical resistance computation and then characterized in this chapter in order to study the in-situ of RSW process. With scanning electron microscope (SEM) images taken on the welded area and the cross-sectional views taken by optical microscope, the microstructure change of material can be correlated with the variation of Z_r closely.

6.1 Experimental Setup

Low carbon steel sheets, 1.0mm thickness were used in this experiment. In order to study the weld nugget growth and microstructure change with respect to welding time, the spot welds were made starting from 0s with an incremental interval of 0.02s (for 50Hz power source). The welding time was set not more than 0.18s. For the result analysis, the SEM images were obtained for 0s, 0.02s, 0.04s and 0.06s welds by focusing on the faying interface of welded area. Optical microscope with magnification factor from 5 to 50 times

was used to obtain the cross-sectional views of weld nugget cut along the centerline of spot weld. These cross-sectional views were taken for 0.08s up to 0.18s welds.

6.2 Correlation between Physical Changes of RSW and Z_r Waveform

Fig. 6.1 showed 3 Z_r waveforms for different welding current to demonstrate the physical change of RSW. It was observed that the Z_r experienced a sharp increment before 0.01s. After the alpha peak, the waveform decreased sharply and finally reached its throat value around 0.02s. Again, it rose up gradually and finally reached the beta peak near to 0.12s for 8.8 kA and 8.2 kA weld. Except from the case of weld expulsion happened about 0.16s for 8.8 kA weld, the waveforms remained about constant until the end of welding process. Additionally, no beta peak was found for 4.5 kA weld because no weld nugget was actually formed after the welding process. In the followings, the physical resistance of RSW was computed and then compared with the Z_r. Furthermore, SEM and microstructure images were presented in order to correlate the microstructure changes with the variation of Z_r.

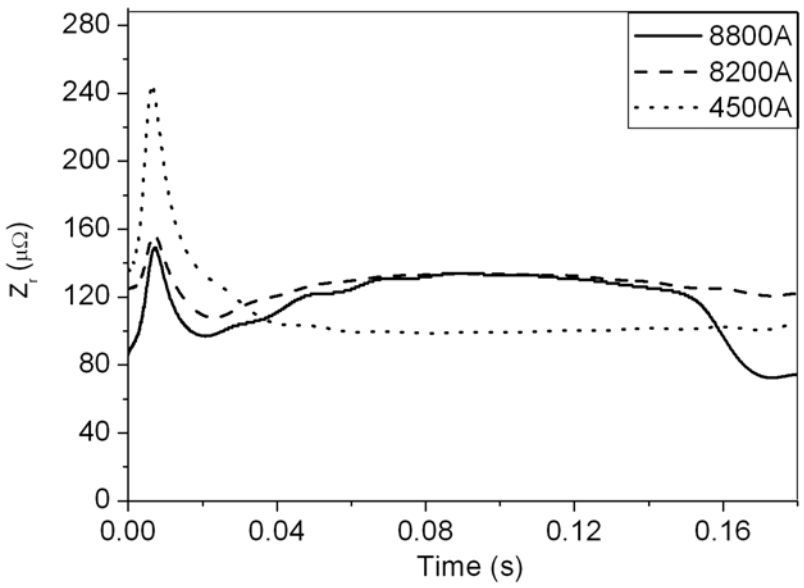

Figure 6.1 Z_r waveforms with different welding current.

As mentioned in Chapter 2, the Z_r represents a series of resistances in the welding process. It consists of the electrode resistance, base material resistance and contact resistances (electrode to sheet and faying interface). The summation of electrode and base resistance is also known as bulk resistance. In theory, the resistivity of a material is sensitive to the change of temperature. Table 6.1 showed the resistivity of low carbon steel at different temperature. Basically, the resistance (R) given by a conductor was proportional to its resistivity and electrical path length but inversed to the cross sectional area of the conductor (see Eq. (2.2)). By considering 1.0mm thickness of low carbon steel with 5mm diameter of the contact area, the resistance of steel (R_{steel}) was computed as 17.2 μΩ at 20ºC. Beside that, the resistance of electrode (R_{copper}) was also calculated as 3.8 μΩ (based on L=35mm; diameter of electrode=20mm; ρ_{copper}=0.017 μΩm). Therefore, the bulk resistance of RSW was equal to 21 μΩ at 0s. If this bulk resistance was compared with the Z_r, it was lower by 70 μΩ. In fact, this huge difference was because the physical

calculation did not include the contact resistance. In other words, the difference between the Z_r and computed bulk resistance will be the contact resistances. At 0.01s, the R_{steel} was calculated as 45 μΩ based on the assumptions made in the followings: 300ºC in temperature; negligible change of the thickness and contact area of the base material. Furthermore, the R_{copper} could be neglected because it was always maintained at low temperature due to the water cooled effect at the electrodes. Using the same method to calculate the contact resistance, it increased to 100 μΩ based on the alpha peak, which was around 150 μΩ.

Table 6.1 Electrical Resistivity of low carbon steel [35].

Temperature (ºC)	Electrical Resistivity (μΩm)
20	0.169
300	0.487
700	0.925
1000	1.167
1300	1.239

According to Fig. 6.1 again, the Z_r dropped to 100 μΩ at 0.02s after the alpha peak. By assuming that the temperature was 700ºC, the R_{steel} was about 100 μΩ. It implied that the contact resistance reduced to zero immediately. This result was drawn based on the observations of SEM images taken on the faying interface of welded area (as shown in Fig. 6.2 and 6.3). At 0s, some tiny gaps were observed together with large flattened surface due to the compression of electrodes (see Fig. 6.2). The flattened surface was

observed to be unchanged but some of the gaps turned to darker color at 0.02s (as shown in Fig. 6.3). In fact, those regions in darker color were the burnt marks due to high temperature. Therefore, the initial melting at faying interface should start from the gaps where the contact resistance was believed to exist. For the flattened surface, it should be considered as short circuit, which the current was free to flow through. Once the elevated temperature (700ºC) was reached, at faying interface, the material was softened and started to deform until the whole contact area was completely flattened. Therefore, the contact resistance was reduced to zero and only the bulk resistance existed.

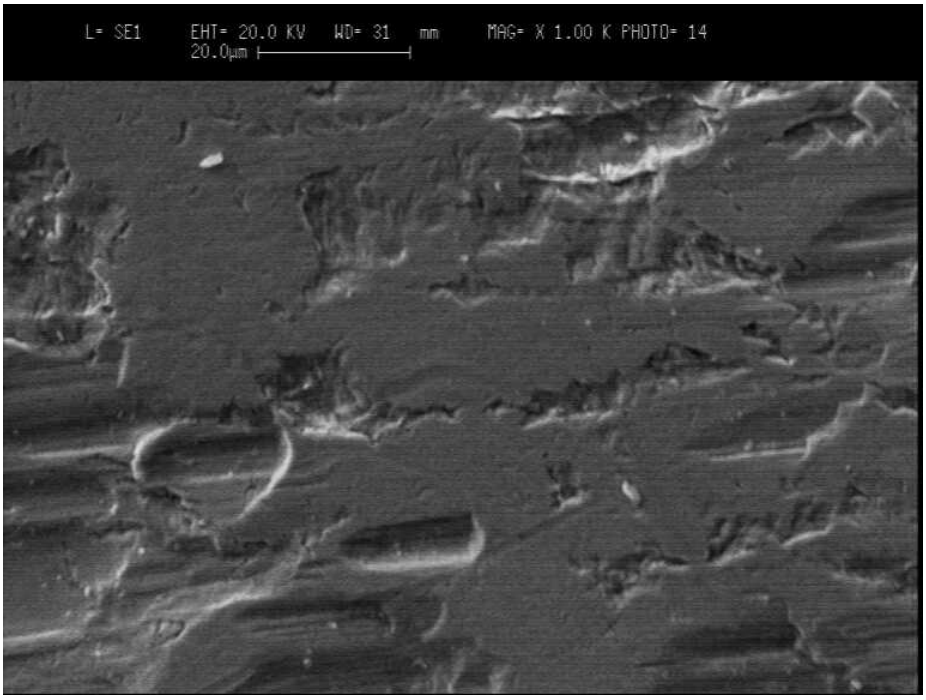

Figure 6.2 SEM image of contact area at faying interface, 0s.

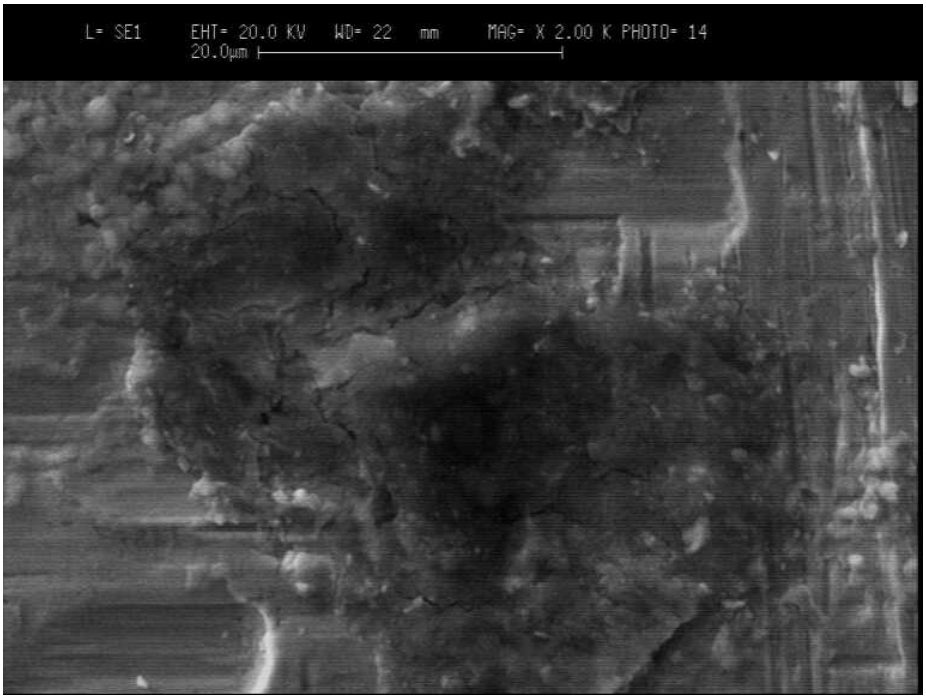

Figure 6.3 Burnt mark found at area in darker color, 0.02s.

Fig. 6.4 showed that the area in darker color actually became bigger as the temperature continued to increase. Assuming that the temperature was 1000ºC at 0.04s, the R_{steel} was computed as 118 μΩ. This value was slightly higher than the Z_r, which was measured as 110 μΩ. The difference of 8 μΩ could be due to the error caused by higher temperature was assumed. Nevertheless, the increment of Z_r was caused by the higher temperature of base material.

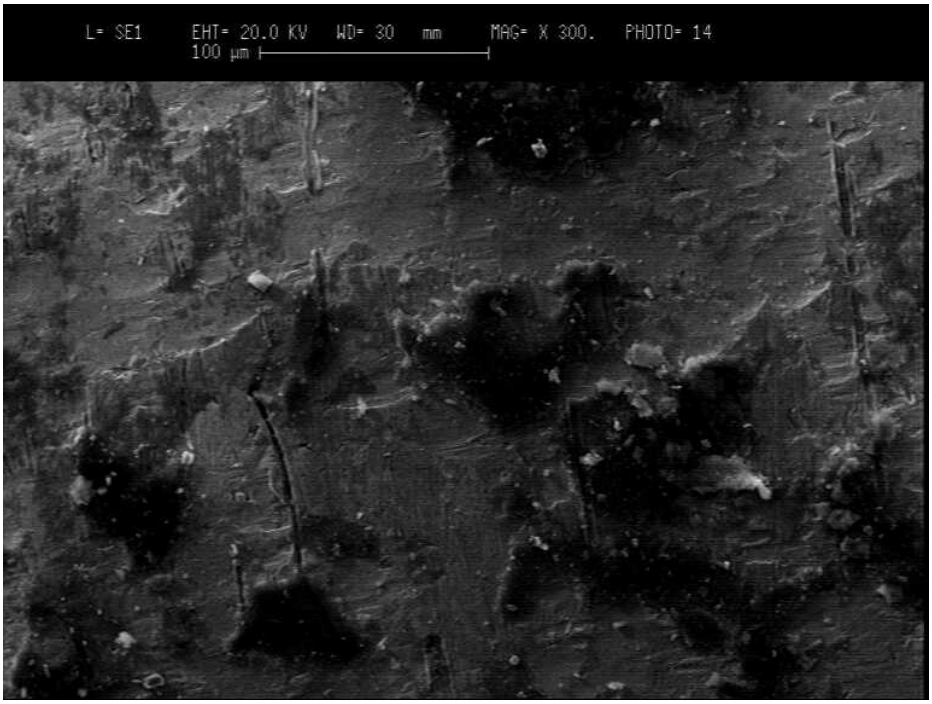

Figure 6.4 Bigger burnt marks found at the contact area, 0.04s.

When the current increased to the pre-set value at 0.06s based on the ramp-up time (60ms), the evidence of melting was found at the contact area (see Fig. 6.5). More metal melting at the center of welded area was observed as compared with those near to the edge of welded area (see Fig. 6.6). This could be due to more heat was conducted away from its edge to the base material and therefore the temperature at the center of welded area was normally higher than the temperature near to the edge of welded area. Therefore, the melting of metal started from the center and then propagated to its surroundings. For bulk resistance, the R_{steel} was gained 126 μΩ based on 1300ºC (melting point). This value was also closed to the Z_r at 130 μΩ with minor error of 4 μΩ. From 0.06s to 0.10s, the Z_r continuously increased to around 135 μΩ, where the beta peak was located. In fact, Fig. 6.7 showed about the Z_r and weld nugget dimensions indicating the history of weld nugget growth. The dimensions were obtained from the measurement of individual weld

nugget. Based on the result shown, the weld nugget started to form around 0.04s and grew rapidly until 0.14s. The increase of Z_r during this period could be due to the resistivity of steel in liquid phase was higher as compared with solid phase [36]. Since the weld nugget had to be in liquid phase, the Z_r rose up proportionally when the volume of molten metal was increasing.

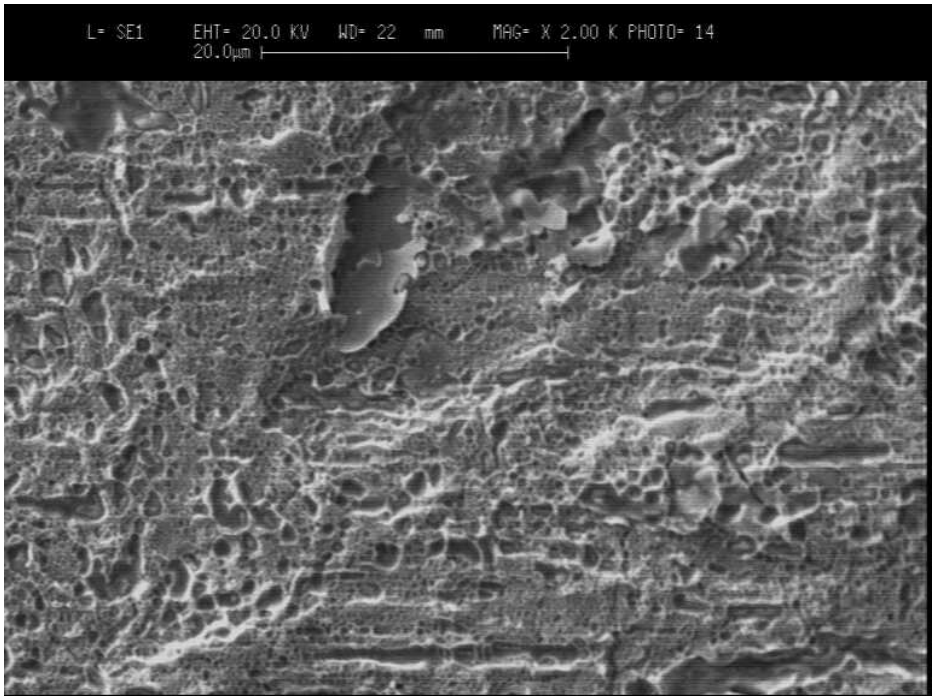

Figure 6.5 Metal melts at center of welded area, 0.06s.

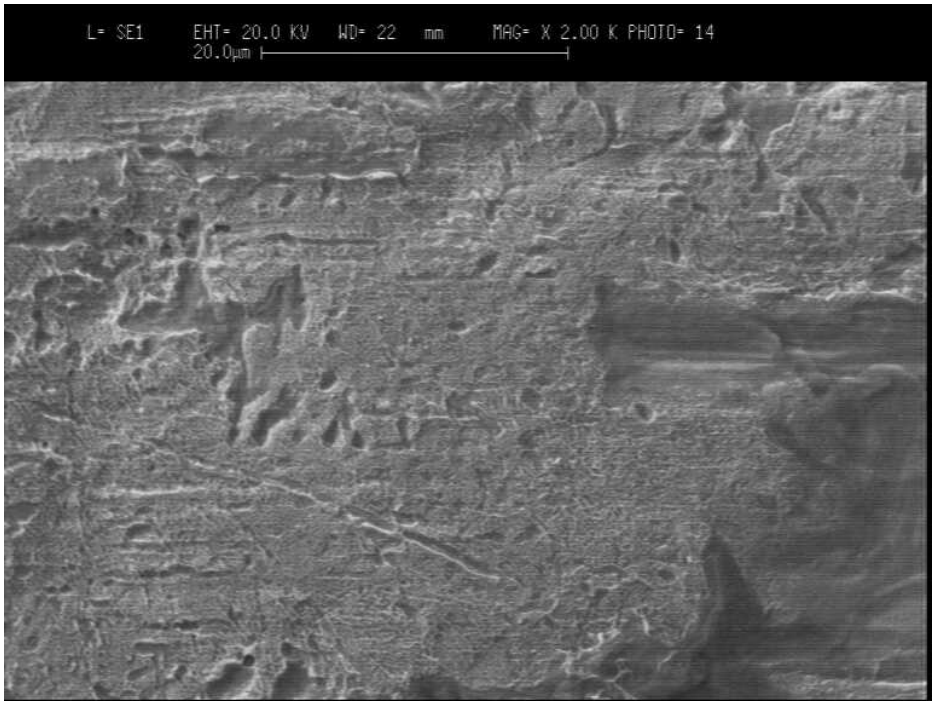

Figure 6.6 Metal melts lesser near to the edge of weld, 0.06s.

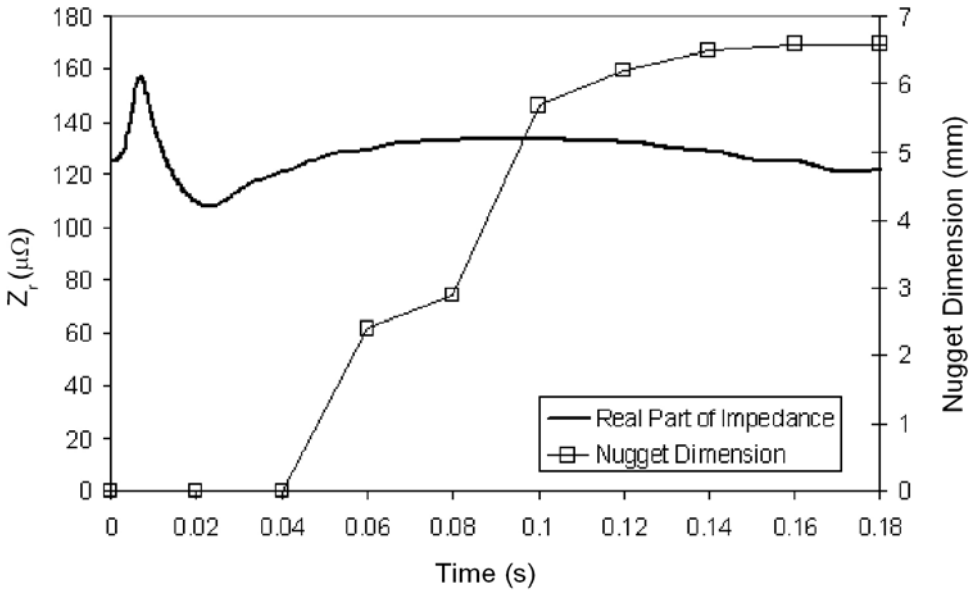

Figure 6.7 Relationship between the Z_r and the weld nugget dimension.

The sudden drop of Z_r was observed near to 0.15s for 8.8 kA weld as a result of weld expulsion. Based on the conclusion drawn in Chapter 5, the weld nugget thickness was measured as 1.75mm and 1.95mm for the weld with and without expulsion. Similarly, both weld nugget dimensions were measured the same value at 6.7mm. From the calculation, the R_{steel} was 61 μΩ against 70 μΩ for the Z_r at 0.18s.

6.3 Characterization of Z_r Waveform

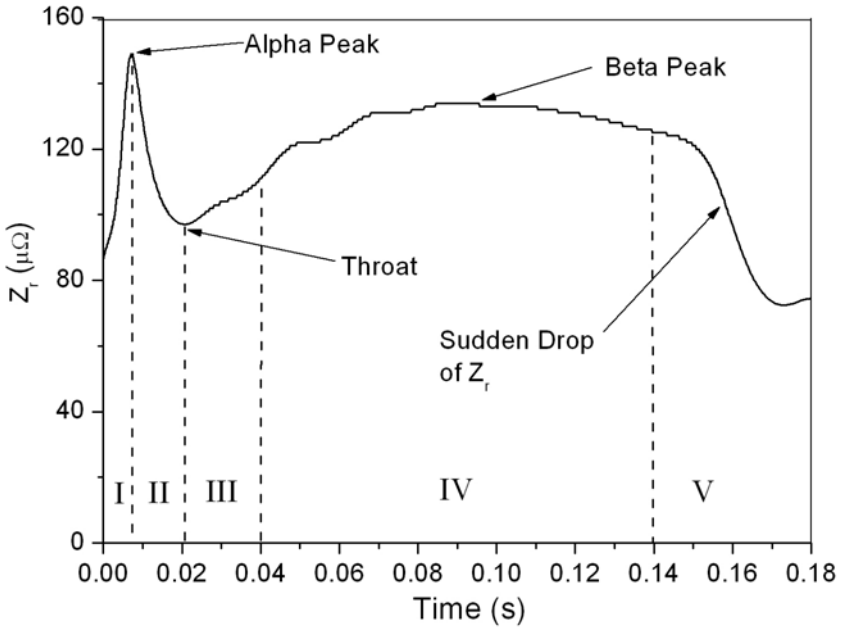

Figure 6.8 Characterization of Z_r.

Based on the results shown above, the Z_r waveform has been confirmed to have good correlation with the physical changes during welding process. Therefore, in order to describe the Z_r waveform according to the microstructure change of RSW process, it can be characterized into the following stages (see Fig. 6.8): (I) initial heating; (II) contact

resistance breakdown; (III) bulk heating; (IV) weld nugget growth and (IV) holding and expulsion. Each stage closely indicates the microstructure changes of RSW with respect to the welding time.

Stage I. At 0s, the bulk resistance is usually low at room temperature but the contact resistance is relatively high. For instance, the contact resistance shall exist only at the tiny gaps due to 2 reasons: (1) the contact resistance caused by the flattened welded area is negligible due to the intimate contact between 2 sheets (see Fig. 6.2); (2) high electrical resistance in the tiny gaps with air because of open circuit connection. When the welding current ramps up with a very fast rate at the beginning, the contact resistance also increase rapidly. Therefore, the sharp increase of Z_r is mainly due to the rapid increase of contact resistance. It pushes the Z_r to reach the alpha peak (first peak) around 0.01s.

In literature studies, this alpha peak could not be clearly identified in the past decades [9]-[13] [37] [38]. There were no research works to report the alpha peak until the small scale resistance spot welding (SSRSW) on thin Ni sheets was carried out and reported by Tan *et al.* [39]. Instead of using AC current, DC current was used for the SSRSW, which implied the possibility of obtaining the alpha peak due to its simple computation by applying the Ohm's Law. The reasons of having difficulty in obtaining the alpha peak for RSW using AC power source are suspected to be caused by the extremely high increasing rate of welding current and the presence of thick surface film at the faying interface. Basically, for a spot weld, the welding time is usually very short but the current is extremely high, which means that the increasing rate of current is very high. For an

example, the increasing rate of welding current for 4.5 kA is 75000A/s based on an average ramp-up time of 60ms. Obviously, the increasing rate of current for 8.8 kA is much higher and rated at 146000 A/s. Despite of having such a high increasing rate of welding current, the results presented in this thesis showing that the alpha peak can be easily obtained by the proposed method. Furthermore, the alpha peak is also not affected by the surface conditions at faying interface. With this break-through technology, it guarantees the alpha peak is obtainable for various welding conditions.

Stage II. After the Z_r reaches its alpha peak, it drops sharply to a relatively low value where the throat is defined. Based on the comparison between the physical calculation and measured Z_r, it reveals that the contact resistance reduces to zero at the throat. The sharp reduction of contact resistance is due to the intimate contact at the faying interface as a result of material softening and deformation after fast heating. Eventually, only bulk resistance of Z_r exists at the throat.

Stage III. Although the Z_r reduces to the throat because the contact resistance reduces to zero, the temperature of base material still continues to increase and hence cause the Z_r to increase again. Without the influence of contact resistance, the Z_r is able to increase gentler as compared with the sharp changes of Z_r in the previous 2 stages because the increase of bulk resistance depends on the temperature of base material only. For the weld nugget growth, it begins at 0.04s (see Fig. 6.7).

Stage IV. This is the most important stage because it describes how the weld nugget grows. At the beginning, the temperature of base material increases to its material melting temperature when the welding current reaches its pre-set value. At the faying interface, the region where tiny gaps are located actually starts to melt. Based on the observations from the microstructure images shown in Fig 6.9 (a) and (b), the weld nugget is able to reach its full penetration into the base material at 0.08s (more than 60% of base material thickness). However, the penetration of weld nugget stops immediately because the heat gain and loss is in balance at the electrode to sheet interface. This heat balance is due to the water cooled effect of electrodes, which remove excessive heat from the base material. From Fig. 6.8, it was observed that the weld nugget still continued to grow in sideway after 0.08s. The reason is because the heat dissipation by conduction from base material and convection to the air is not efficient as compared with the water cooled at the electrode to sheet interface. Therefore, the weld nugget growth is not interrupted so long as the welding current continues to flow and the heat balance is not achieved.

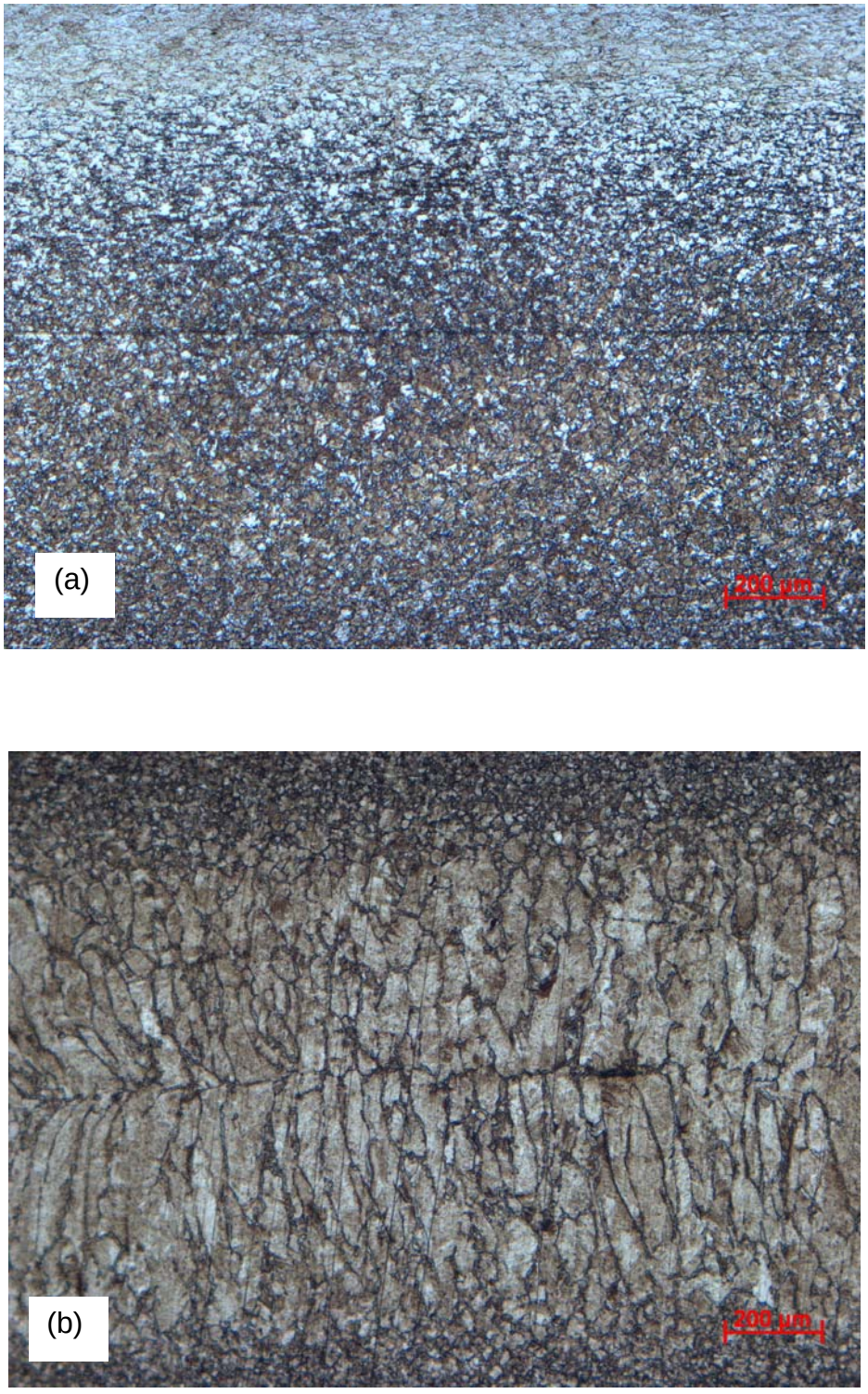

Figure 6.9 Cross sectional views along the center of weld, (a) 0.06s; (b) 0.08s.

During the weld nugget growth, more material is transformed from solid to liquid phase. As mentioned earlier, the electrical resistivity is even higher if it is in liquid phase. Therefore, the increase of Z_r is dependent on the weld nugget growth because the more material turns into liquid phase, the higher the Z_r will be. At the beta peak, the Z_r reaches its second maximum point and remains about constant till the end of welding process. Due to the heat balance is finally achieved between the weld nugget and base material, the fusion of material stops and subsequently the increase of Z_r also rest at its beta peak. This heat balance is retained until the end of welding process so that the weld nugget with correct dimension is ensured after the rapid solidification of the fused material. In the case of no weld nugget is formed after weld, it is expected that the beta peak will be missing as shown in Fig. 6.1.

Stage V. In case of weld expulsion, the Z_r encounters a sudden drop near to the end of welding process. The reason of this sudden drop has already been mentioned in Chapter 5, which is caused by the low pressure. However, it was observed that the excessive high welding current also caused the expulsion to happen (see Fig. 6.1). The sudden drop of Z_r happened around 0.15s for 8.8 kA weld, which was associated with the observation of light weld expulsion during the welding process. For instance, the material can fuse more than its allowable size because higher welding current actually generates more heat to the material. Therefore, the electrodes are not able to hold the excessive molten metal and then it is ejected to its surroundings.

CHAPTER 7

CONCLUSIONS AND FUTURE PROSPECTS

This chapter is aimed to summarize the works and findings of this research and also provide suggestions for future investigations and developments.

7.1 Summary of Results

The need for an automated and real time quality monitoring system becomes more crucial due to the higher requirements for quality control of RSW. From the literature study and industrial surveys, it was realized that most of the existing monitoring system cannot deliver satisfactory quality assurance for RSW because they either sacrificed the productivity, accuracy and cost effectiveness or had low efficiency and robustness. In this research, a new NDT monitoring method was implemented by adopting the input electrical impedance as monitoring signature for RSW. In Chapter 3, an ANN was used to confirm its capability in real-time monitoring of weld quality. 6 feature points were selected from the Z_r waveforms and then input to a 6-5-1, Feed Forward Back Propagation Neural Network for weld quality classification. After the training and verification of ANN was done, the outputs showed that it could distinguish the good or bad welds by mean of weld strength with 100% accuracy. Furthermore, the outcome can be displayed almost instantly after each spot weld is successfully made because the

processes of taping signals, impedance calculation and weld quality classification are completed in millisecond. Based on the results shown above, a conceptual design was introduced in order to realize the proposed system.

In order to further understand how the variation of Z_r waveform is correlated with the change of operating parameters and process conditions, 1 abnormal process condition: (angled weld) and 3 operating parameters (pressure, welding current and electrode) are studied to investigate their effects on the Z_r waveform in Chapter 5. In fact, the waveform was observed to deviate significantly for the changes of angled weld, pressure, welding current and tip surface conditions of electrode. For the welding strength, only low welding current and electrode with side damage on its tip surface were tested for bad weld. Therefore, the weld quality determined by the welding strength can be correlated with the features of Z_r waveform.

In Chapter 6, the Z_r waveform also showed its capability for in-situ study of RSW. The microstructure changes of material during the welding process was clearly demonstrated by the variation of Z_r waveform, which provided a more accurate and powerful monitoring signature for RSW beside dynamic resistance. Some important findings such as the alpha peak, throat, beta peak and sudden drop of Z_r have also been discussed in detail. The results also showed that the missing of alpha peak, which was almost impossible to obtain by the old dynamic resistance method, could be easily solved by using this method. For the throat, it indicated that the contact resistance at faying interface was reduced to zero. Therefore, it can be used to check the total thickness of a

lap-joint because it can be easily computed by the Z_r only at the throat. After the throat, the growth of weld nugget was found to be related to the slope of Z_r from throat to beta peak. It also revealed that the seriousness of weld expulsion could be reflected by the time occurrence of sudden drop of Z_r. Lastly, in order to describe better about the dynamic behavior of RSW, the Z_r waveform was characterized into 5 stages: (I) initial heating; (II) contact resistance breakdown; (III) bulk heating; (IV) weld nugget growth and (IV) holding and expulsion.

7.2 Future Direction and Developments

Based on the ANN result and conceptual design of this proposed system, it shall continue with the prototyping and testing process of the system so that it can be further improved in order to realize the commercialization of this system. It is believed that the features of this system such as fully automation, high accuracy, good robustness and easy to operate will greatly benefit to the industry. However, more appropriate feature points of Z_r such as the initial Z_r at 0s, alpha peak and etc shall be selected and tried out for the ANN not only to improve its accuracy and efficiency but also to explore more possibilities of the system in diagnosing the defects of weld like small nugget, loose weld, bad through and burnt weld.

The imaginary part of impedance (Z_x), beside Z_r, is also obtained together during impedance calculation. Based on the literature study, it was always considered as inductive noise in the RSW system because obtaining the pure resistance was almost

impossible with the existence of this reactance. However, by using the proposed method, the resistance and reactance can be obtained together and yet they do not interfere into each other. In other words, the pure resistance and reactance of the RSW system are obtained simultaneously. Since the impedance is such an important system property of RSW, the Z_x shall be able to provide rich information about the RSW system also as compared with the Z_r. Some preliminary study of Z_x was done but the result was not presented in this thesis. Therefore, more research work can be done in order to find out more about the Z_x.

Developing a mathematic model for RSW based on the impedance is a possible way to enhance the knowledge of impedance for RSW. It has been found that the slope of Z_r starting from throat to beta peak is related to the weld nugget growth. Therefore, a reversed two-port network model [40] is proposed to formulate the coupling of thermal heat and impedance. The thermal heat (temperature and heat flow) will be put at the input port of the model while the impedance is considered at the output port. Similarly, the preliminary study in solving the thermal coupling problem has been done but it was not covered in this thesis too.

By tapping the voltage probe at different location, it was found that the corresponding impedance by its nature can represent the dynamic behavior of the prescribed system also. For an example, taping the voltage probe at the upper electrode and the top metal sheet can reflect the physical changes of upper electrode to top sheet interface only. Therefore, rich information about the tip surface conditions of upper electrode should be able to

obtain. Furthermore, by taping the voltage probe to 2 adjacent metal sheets, the result can be used to study the multiple lapped joints with different thickness of metal sheets more efficiently.

LIST OF PUBLICATIONS

1. YokeRung Wong, Shih-Fu Ling & MengKit Lee. Investigation of Effects of Mis-aligned Spot Welding to Weld Strength. *Proceedings of the First South-East Asia International Institute of Welding Congress*, November 2006, pp. 352-357.

2. Shih-Fu Ling, LiXue Wan & YokeRung Wong. Input Electrical Impedance as Quality Monitoring Signature for Resistance Spot Welding. **To be submitted**.

REFERENCES

[1] Milner D.R. Introduction to Welding and Brazing. Pergamon Press, 1968.

[2] Robert Scharff. & Dave Caruso. Complete Automotive Welding Metals and Plastics. Delmar, 1990.

[3] R. J. Bowers, C.D. Sorensen & T. W. Eagar. Electrode Geometry in Resistance Spot Welding. *Welding Journal*, February 1990, pp. 45-51.

[4] Quanfeng Song, Wenqi Zhang & Niels Bay. An Experimental Study Determines the Electrical Contact Resistance in Resistance Welding. *Welding Journal*, May 2005, pp. 73-76.

[5] N. T. Williams & J. D. Parker. Review of Resistance Spot Welding of Steel Sheets. *International Materials Reviews*, 49(2), 2004, pp. 45-75.

[6] K. S. Yeung & P. H. Thornton. Transient Thermal Analysis of Spot Welding Electrodes. *Welding Journal*, January 1999, pp. 1-6.

[7] S. Fukumoto, I. Lum, E. Biro, D. R. Boomer & Y. Zhou. Effects of Electrode Degradation on Electrode Life in Resistance Spot Welding of Aluminum Alloy 5182. *Welding Journal*, 82(11), November 2003, pp. 307-312.

[8] Howard B. Cary. Modern Welding Technology 4th ed. Prentice Hall, 1998.

[9] Dickinson D. W., Franklin J. E. & Stanya A. Characterization of Spot Welding Behavior by Dynamic Electrical Parameter Monitoring. *Welding Journal*, 59(6), June 1980, pp. 170-176.

[10] Savage W. F., Nippes E. F. & Wassell F. A. Dynamic Contact Resistance of Series Spot Welds. *Welding Journal*, 57(2), February 1978, pp. 43-50.

[11] Gedeon S. A., Sorensen C. D., Ulrich K. T. & Eagar T. W. Measurement of Dynamic Electrical and Mechanical Properties of Resistance Spot Welds. *Welding Journal*, 66(12), December 1987, pp 378-385.

[12] Y. Cho & S. Rhee. Primary Circuit Dynamic Resistance Monitoring and its Application to Quality Estimation during Resistance Spot Welding. *Welding Journal*, 81(6), June 2002, pp. 104-111.

[13] S. C. Wang & P. S. Wei. Modeling Dynamic Electrical Resistance during Resistance Spot Welding. *Transactions of the ASME. Journal of Heat Transfer*, 123(3), June 2001, pp. 576-585.

[14] Specification for Resistance Spot Welding of Uncoated and Coated Low Carbon Steel. *British Standard*, BS 1140:1993, Section 10.2.

[15] Adams T. Nondestructive Evaluation of Resistance Spot Welding Variables Using Ultrasound *Welding Journal*, 64(6), June 1985, pp. 27-28.

[16] Waschkies E. Process-integrated Resistance Spot-welding Testing Using Ultrasonic Techniques. *Welding in the World*, 39(6), November-December 1997, pp. 345-350.

[17] Wei Li, S. Jack Hu & Jun Ni. On-line Quality Estimation in Resistance Spot Welding. *Journal of Manufacturing Science and Engineering*, 122, August 2000, pp. 511-512.

[18] Yongjoon Cho & Sehun Rhee. New Technology for Measuring Dynamic Resistance and Estimating Strength in Resistance spot Welding. *Measurement Science & Technology*, 11(8), August 2000, pp. 1173-1178.

[19] Farson D. F., J. Z. Chen, Ely K. & Frech T. Monitoring Resistance Spot Nugget Size by Electrode Displacement. *Transaction of the ASME, Journal of Manufacturing Science and Engineering*, 126(2), May 2004, pp. 391-394.

[20] Li YongBing, Xu Jun, Chen GuanLong & Lin ZhongQin. Real-time Measuring System Design and Application of Thermal Expansion Displacement during Resistance Spot Welding Process. *Proceedings of SPIE-The International Society for Optical Engineering, ICMIT 2005, 6041: Information Systems and Signal Processing*, February 2006, pp. 60411T-1-6.

[21] Primoz Podrzaj, Ivan Polajnar, Janez Diaci & Zoran Kariz. Estimating the Strength of Resistance Spot Welds Based on Sonic Emission. *Science and Technology of Welding and Joining*, 10(4), 2005, pp. 399-405.

[22] Rodger E. Ziemer, William H. Tranter & D. Ronald Fannin. Signals and Systems: Continuous and Discrete, 3rd ed. Macmillan, 1993.

[23] Richard S. Figliola & Donald E. Beasley. Theory and Design for Mechanical Measurements, 2nd ed. John Wiley & Sons, Inc., 1995.

[24] M. Zhou, S. J. Hu & H. Zhang. Critical Specimen Sizes for Tensile-shear Testing of Steel Sheets. *Welding Journal*, 78(9), September 1999, pp. 305-313.

[25] Wei Li, Shaowei Cheng, S. Jack Hu & Justin Shriver. Statistical Investigation on Resistance Spot Welding Quality Using a Two-State, Sliding-Level Experiment. *Transaction of the ASME, Journal of Manufacturing Science and Engineering*, 123, August 2001, pp. 513-520.

[26] Shih Fu Ling & Lixue Wan. Monitoring a Spot Welding Process via Electrical Input Impedance. *SEM IX International Congress On Experimental Mechanics*, June 2000, pp. 348-351.

[27] Shih-Fu Ling, Jingen Luan, XiangChao Li & WendyLee Ang. Input Electrical Impedance as Signature for Nondestructive Evaluation of Weld Quality during Ultrasonic Welding of Plastics. *NDT&E International*, 39(1), January 2006, pp. 13-18.

[28] LianYu Fu, Shih-Fu Ling & Ching-Huan Tseng. On-line Breakage Monitoring of Small Drills with Input Impedance of Driving Motor. *Mechanical Systems and Signal Processing*, 21(1), January 2007, pp. 457-465.

[29] Shih-Fu Ling, Dong Zhang, Sung Yi & Say Wee Foo. Real-time Quality Evaluation of Wire Bonding Using Input Impedance. *IEEE Transactions on Electronics Packaging Manufacturing*, 29(4), October 2006, pp. 280-284.

[30] Duda R.O., Hart P.E. & Stork D.G. Pattern Classification, 2nd ed. Wiley, 2001.

[31] Statistics Toolbox For Use with Matlab® User's Guide Version 5. The MathWorks Inc, 2004.

[32] Dhandapani S., Bridges M. & Kannatey-Asibu E. Jr. Nonlinear Electrical Modeling for the Resistance Spot Welding Process. *Proceedings of the 1999 American Control Conference*, 1(1), June 1999, pp. 182-186.

[33] Davalo E. & Niam P. Neural Network. the Macmillan Press Ltd, 1991.

[34] Y. R. Wong, Shih-Fu Ling & M. K. Lee. Investigation of Effects of Mis-aligned Spot Welding to Weld Strength. *Proceedings of the First South-East Asia International Institute of Welding Congress*, November 2006, pp. 352-357.

[35] Philip D. Harvey. Engineering Properties of Steel. American Society for Metals, 1985.

[36] Tslaf A. Combined Properties of Conductors. Elsevier, 1981.

[37] Williams N.T. & Parker J.D. Review of Resistance Spot Welding of Steel Sheets. *International Materials Reviews*, 49(2), April 2004, pp. 45-75.

[38] Wei Li. Modeling and On-line Estimation of Electrode Wear in Resistance Spot Welding. *Transactions of the ASME. Journal of Manufacturing Science and Engineering*, 127(4), November 2005, pp. 709-717.

[39] W. Tan, Y. Zhou, H. W. Kerr & S. Lawson. A study of Dynamic Resistance during Small Scale Resistance Spot Welding of Thin Ni Sheets. *Journal of Physics D: Applied Physics*, 37(14), July 2004, pp. 1998-2008.

[40] John P. Bentley. Principles of Measurement Systems, 3rd ed. Prentice Hall, 1995.

Appendix A

R.W.M.A. Standard

Table of RSW conditions for mild steel sheets

Sheet thickness	Electrode tip		Pitch	Lap	CLASS A Best condition					CLASS B Medium condition					CLASS C Ordinary condition				
	d	D			Time	Pressure	Current	Nugget Dia	Strength ±14%	Time	Pressure	Current	Nugget Dia	Strength ±17%	Time	Pressure	Current	Nugget Dia	Strength ±20%
mm	mm		mm		∞	Kgf	A	mm	kg	∞	kgf	A	mm	kg	∞	kgf	A	mm	kg
0.25	3.2	10	6	10	4	90	4000	3.3	105	5	60	3700	3.0	90	15	30	3000	2.8	70
0.4	3.2	10	6	10	5	115	5200	4.0	180	8	75	4500	3.6	160	20	40	3500	3.3	125
0.5	3.5	10	9	11	6	135	6000	4.3	240	10	90	5000	4.0	210	24	45	4000	3.6	175
0.6	4.0	10	10	11	7	150	6600	4.7	300	12	100	5500	4.3	280	26	50	4300	4.0	225
0.8	4.5	10	12	11	8	190	7800	5.3	440	15	125	6500	4.8	400	30	60	5000	4.6	355
1.0	5.0	13	18	12	10	225	8800	5.8	610	20	150	7200	5.4	540	36	75	5600	5.3	530
1.2	5.5	13	20	14	12	270	9800	6.2	780	23	175	7800	5.8	680	40	85	6100	5.5	650
1.4	6.0	13	23	15	14	305	10600	6.6	930	26	210	8500	6.3	850	46	100	6600	5.9	780
1.6	6.3	13	27	16	16	360	11500	6.9	1060	30	240	9100	6.7	1000	50	115	7000	6.3	920
1.8	6.7	16	31	17	18	410	12500	7.4	1300	33	275	9700	7.1	1180	54	130	7500	6.7	1100
2.0	7.0	16	35	18	20	470	13300	7.9	1450	36	300	10300	7.6	1370	58	150	8000	7.1	1305
2.4	7.8	16	40	20	24	580	15000	8.6	1850	44	370	11300	8.4	1770	65	180	8600	7.9	1685
2.8	8.5	16	45	21	28	700	16200	9.4	2380	52	430	12100	9.2	2300	72	220	9400	8.9	2180
3.2	9.0	16	50	22	30	820	17500	10.2	3130	60	520	12900	9.9	2940	78	260	10000	9.4	2790
3.6	10.3	22	57	29	41	930	18200	11.2	3880	72	560	13600	10.7	3600	102	280	10600	10.2	3380
4.0	11.1	22	67	32	50	1030	18900	11.9	4450	88	640	14100	11.4	4200	125	320	11000	10.7	3900
4.3	11.1	22	76	38	61	1120	19600	12.9	5250	107	720	14700	12.2	4780	152	360	11400	11.4	4420

Sheet thickness	Electrode tip		Pitch	Lap	CLASS A Best condition					CLASS B Medium condition					CLASS C Ordinary condition				
	d	D			Time	Pressure	Current	Nugget Dia	Strength ±14%	Time	Pressure	Current	Nugget Dia	Strength ±17%	Time	Pressure	Current	Nugget Dia	Strength ±20%
mm	mm		mm		∞	Kgf	A	mm	kg	∞	kgf	A	mm	kg	∞	kgf	A	mm	kg
4.7	11.9	22	83	41	73	1260	20200	13.7	6000	128	800	15300	12.9	5460	182	400	11750	11.9	5030
5.1	12.7	22	89	45	84	1320	20900	14.7	6690	147	880	15900	13.7	6080	210	440	12200	12.7	5600
5.5	13.5	22	98	48	95	1460	21800	15.5	7300	166	970	16450	14.5	6680	237	490	12500	13.2	6120
5.9	13.5	22	108	54	106	1560	22300	16.5	7980	186	1040	17000	15.2	7350	265	520	12900	14.0	6700
6.4	15.1	25	114	57	116	1710	23000	17.3	8570	204	1140	17600	16.0	7940	290	570	13200	14.5	7240
6.6	15.1	25	121	60	127	1850	23600	18.0	9200	222	1230	18100	16.8	8500	318	620	13600	15.0	7780
7.0	15.1	25	133	67	140	1960	24400	19.1	9850	245	1300	18700	17.5	9250	350	660	14000	15.7	8370
7.9	16.9	25	146	73	162	2200	25700	20.2	10900	284	1480	19800	18.8	10400	405	740	14800	17.0	9440

1. The material shown in this table that is subject to welding shall be a pickled and lightly lubricated mild steel sheet with a tensile strength ranging from 294 N/mm^2 to 314 N/mm^2, and there shall be no black scale, grease, oxide, paint, dust, etc. on the surface of the material to be welded.
2. Electrode material shall be R.W.M.A. Class2, and the tip of the electrode shall be as shown in attached Figure, (a). The tolerance of dΦ shall be ±0.4 mm.
3. The minimum pitch indicates the lowest value at which the shunt effect of the neighbouring spot can be disregarded. (When welding within this pitch, it is necessary to increase the current to an appropriate value in consideration of the shunt effect.)
4. The minimum lap is the L value shown in attached Figure (b).
5. The welding time indicates the number of cycles at a power-supply frequency of 60 Hz. Accordingly, 10 cycles corresponds to 1/6 sec, and when welding is performed at a power-supply cycle f 50, the welding time must be set to 5/6 of the value shown in this table.
6. The strength is the sharing strength per point, and the allowance represents percentage of an unsharing strength.
7. When welding a workpiece consisting of two sheets of different thicknesses, the welding conditions shall be in accordance with the thinner of the two. (Where the thickness ratio of the pair of sheets for welding shall be within 1:3 and the convex electrode shall be on the side of sheet thickness.) Further, the welding condition given in this table may also apply to welding of four-lapped sheet. (Where the total thickness of four sheets shall be within four times the thickness of one sheet.)

Attached Figure (a)

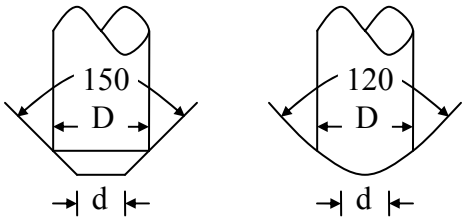

Thickness <3.2mm Thickness >3.6mm

Attached Figure (b)

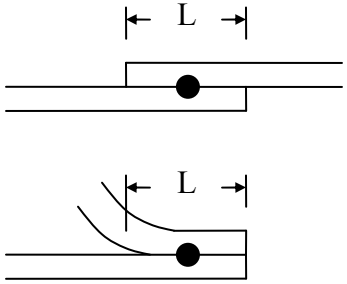

Appendix B

Instron Material Testing Equipment, 5569 Series

Capacity	Speed Range	Load Accuracy
50kN	0.001-500 mm/min	±0.5%

Appendix C

Kimura Welding Machine SW-505 with Miyachi Timer CT-110B

Rated Frequency	Rated Capacity	Maximum Current Output	Other
50Hz	75KVA	19,000 A	Water cooled

Appendix D

Experimental Setup

Equipment Name	Model No
Current probe, (high current)	AmpFlex, Flexible AC Current Probes, 10000-24-2-0.1
Low Pass Filter	K-H 3940
Scope	Nicolet, Integra 40

Appendix E

DAQ System Process Flowchart

Stage A Process Flowchart (Computed by Matlab™)

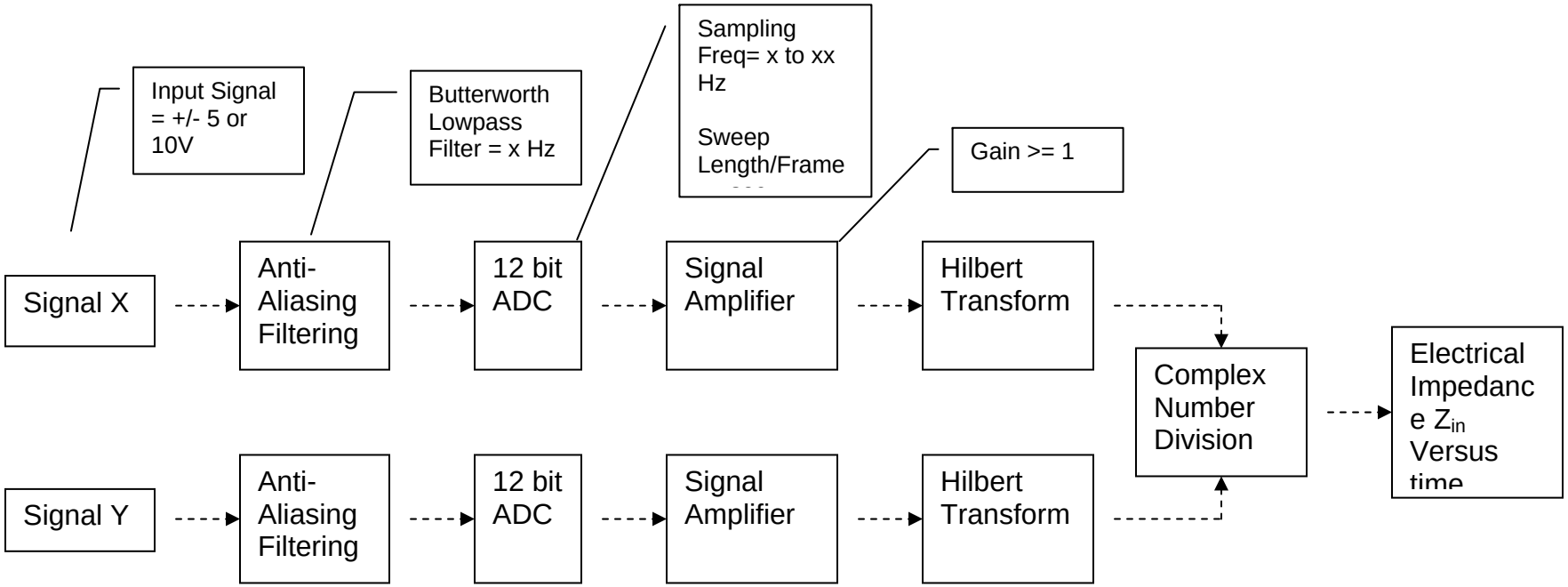

Stage B Process Flowchart (Computed by Matlab™)

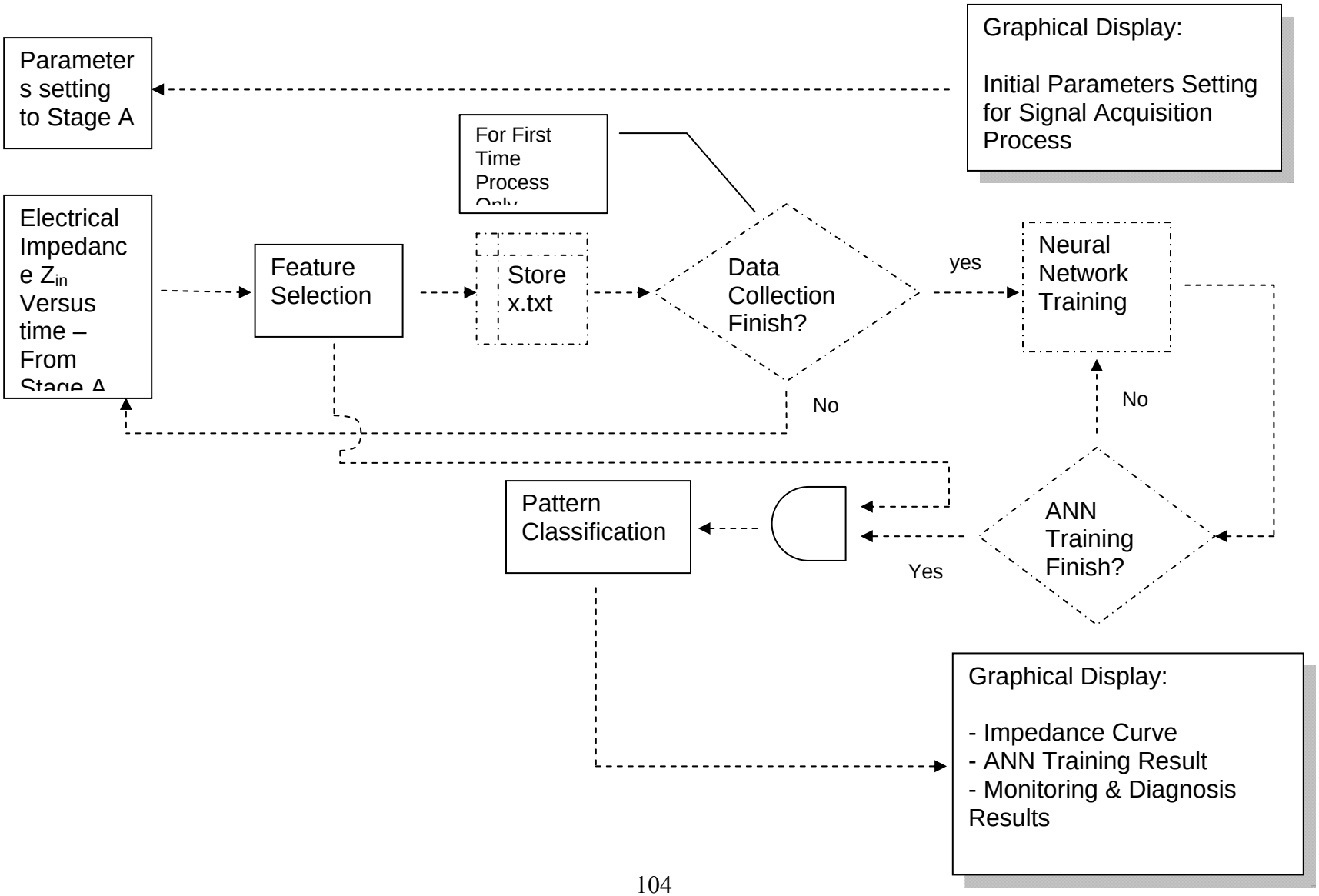

Appendix F

Tensile Shear Testing Results (1.2mm Thickness)

No.	Current Setting (A)	Welding Strength (N)	Welding Quality (> 6700N, good weld)
1	9800	8240	Good
2	9800	8200	Good
3	9800	8300	Good
4	9500	8130	Good
5	9500	8150	Good
6	8300	6120	Bad
7	8000	5230	Bad
8	7000	2320	Bad
9	6000	213	Bad
10	5000	124	Bad